

Global Dust Cycle and Direct Radiative Effect in E3SM Version 1: Impact of Increasing Model Resolution

Yan Feng¹, H Wang², P J Rasch², K Zhang², W Lin³, Q Tang⁴, S Xie⁴, D S Hamilton⁵, N Mahowald⁵, and H Yu⁶

¹Argonne National Laboratory

²Pacific Northwest National Laboratory

³Brookhaven National Laboratory

⁴Lawrence Livermore National Laboratory

⁵Cornell University

⁶NASA Goddard Space Flight Center

November 23, 2022

Abstract

14 15 Key Points: 16 (1) E3SMv1 captures spatial and temporal variability in the observed dust aerosol optical 17 depth, but underestimates long-range transport. 18 (2) The net direct radiative effect of dust simulated by E3SMv1 is -0.42 Wm⁻² with a smaller 19 longwave warming than other recent studies. 20 (3) In addition to emission, dry removal of dust are highly sensitive to the increase of 21 horizontal or vertical model resolution. 22 23 24

1 **Global Dust Cycle and Direct Radiative Effect in E3SM Version 1:**
2 **Impact of Increasing Model Resolution**
3

4 **Y. Feng¹, H. Wang², P. J. Rasch^{2,7}, K. Zhang², W. Lin³, Q. Tang⁴, S. Xie⁴, D.S. Hamilton⁵,**
5 **N. Mahowald⁵, and H. Yu⁶**

6 ¹Environmental Science Division, Argonne National Laboratory, Lemont, IL 60439, USA

7 ²Pacific Northwest National Laboratory, Richland, WA 99352, USA

8 ³Brookhaven National Laboratory, NY 60439, USA

9 ⁴Lawrence Livermore National Laboratory, Livermore, CA 94550, USA

10 ⁵Cornell University, Ithaca, NY 14853, USA

11 ⁶NASA Goddard Space Flight Center, Greenbelt, MD 20771, USA

12 ⁷University of Washington, Seattle, WA, USA

13
14 Corresponding author: Yan Feng (yfeng@anl.gov)

15
16 **Key Points:**

- 17 (1) E3SMv1 captures spatial and temporal variability in the observed dust aerosol optical
18 depth, but underestimates long-range transport.
- 19 (2) The net direct radiative effect of dust simulated by E3SMv1 is -0.42 Wm^{-2} with a smaller
20 longwave warming than other recent studies.
- 21 (3) In addition to emission, dry removal of dust are highly sensitive to the increase of
22 horizontal or vertical model resolution.

Abstract

Quantification of dust aerosols in Earth System models (ESMs) has important implications for water cycle and biogeochemistry studies. This study examines the global life cycle and direct radiative effects (DRE) of dust in the U.S. Department of Energy's Energy Exascale Earth System Model version 1 (E3SMv1), and the impact of increasing model resolution both horizontally and vertically. The default 1° E3SMv1 captures the spatial and temporal variability in the observed dust aerosol optical depth (DAOD) reasonably well, but overpredicts dust absorption in the shortwave. Simulations underestimate the dust vertical and long-range transport, compared with the satellite dust extinction profiles. After updating dust refractive indices and correcting for a bias in partitioning size-segregated emissions, both shortwave cooling and longwave warming of dust simulated by E3SMv1 are increased and agree better with other recent studies. The estimated net dust DRE of -0.42 Wm^{-2} represents a stronger cooling effect than the observationally based estimate -0.2 Wm^{-2} (-0.48 to $+0.2$), due to a smaller longwave warming. Constrained by a global mean DAOD, model sensitivity studies of increasing horizontal and vertical resolution show strong influences on the simulated global dust burden and lifetime primarily through the change of dust dry deposition rate; there are also remarkable differences in simulated spatial distributions of DAOD, DRE and deposition fluxes. Thus, constraining the global DAOD is insufficient for accurate representation of dust climate effects, especially in transitioning to higher- or variable-resolution ESMs. Better observational constraints of dust vertical profiles, dry deposition, size and longwave properties are needed.

45

Plain Language Summary

46

Dust aerosols affect Earth's climate through a myriad of pathways interacting with the global energy budget, atmospheric chemistry and biogeochemical cycles. It is critical for Earth system models to capture the global life cycle of dust aerosols for realistically quantifying the impact of climate change. As part of development of the U.S. Department of Energy's Energy Exascale Earth System Model Version 1 (E3SMv1), this study examines the representation of global dust life cycle and direct radiative effects in the recently released E3SMv1, resulting from both model physics improvements and increased model resolution. We find that the E3SMv1 model captures the spatial and temporal variations in the observed dust aerosols reasonably well, but underestimates the amount of dust advecting from desert sources to remote regions and from the ground to the upper atmosphere. Based on the model projection, dust aerosols insert a stronger cooling effect on Earth than previously estimated, after we use a better representation of dust particle size and absorption of sunlight. In addition, we show that not only dust generation but also removal and vertical transport of dust are highly sensitive to the model mesh size, thus need to be quantified in development of higher resolution models.

62

63 **1 Introduction**

64 Dust aerosols affect Earth's climate through direct and indirect impacts on the global
65 energy budget. They can directly attenuate the incoming shortwave (SW) solar radiation by
66 scattering and absorption (Tegen et al., 1996), and indirectly, modify cloud microphysical
67 properties by acting as ice nuclei (DeMott et al., 2003) and cloud condensation nuclei (Rosenfeld
68 et al., 2001), which change cloud albedo and thus affect the radiation balance. Despite being weak
69 SW absorbers as individual particles, the abundant mass of dust in the atmosphere could cause a
70 atmospheric heating that leads to changes of the lower troposphere thermal structure, cloud cover
71 and liquid water path (Amiri-Farahani et al., 2017; Doherty & Evan, 2014). Additionally, dust
72 absorbs in the infrared and longwave (LW) spectra due to unique characteristics of its mineral
73 components (Sokolik et al., 1998). The LW effect of dust tends to cool the dust-laden layer and
74 warm the air below, offsetting its direct SW warming effect within the atmosphere and cooling
75 effect at the surface (Zhu et al., 2007). When deposited on snow or ice, dust particles can accelerate
76 snowmelt by increasing the SW absorption similar to the effect of black carbon (Painter et al.,
77 2012; Skiles et al., 2012). By perturbing the radiation energy balance, dust aerosols have further
78 impacts on the large-scale general circulation (Evan et al., 2011; Lau et al., 2009; Miller et al.,
79 2004) and regional precipitation (Solmon et al., 2015; Vinoj et al., 2014; C. Zhao et al., 2012; C.
80 Zhao et al., 2011).

81 Other climate effects of dust occur through biogeochemical feedbacks and interactions with
82 atmospheric chemistry. Dust particles deposited to the ocean surface are a major source of the
83 essential micronutrients such as iron, which stimulate phytoplankton growth and nitrogen fixation
84 in the high-nutrient low-chlorophyll sea waters (Jickells et al., 2005). Iron-enrichment driven by
85 increased dust deposition could enhance the ocean uptake of atmospheric carbon dioxide
86 (Hamilton et al., 2020), which is equivalent to inducing a negative climate forcing (Mahowald,
87 2011). Dust deposition also replenishes nutrient losses from soil and affects the health of terrestrial
88 ecosystems (Yu, Chin, Yuan, et al., 2015). Additionally, dust plays a role in the gas-phase
89 atmospheric chemistry and secondary aerosol formation by providing reactive surfaces for
90 heterogeneous reactions with gaseous precursors (Dentener et al., 1996; Feng & Penner, 2007; C.
91 Liu et al., 2013). Thus, it is critical for Earth system models (ESMs) to simulate the global life
92 cycle of dust aerosols for both realistically quantifying the global energy balance and improved
93 understanding of land-atmosphere-ocean couplings and feedbacks.

94 However, there are large differences in dust simulations among ESMs and between models
95 and observations. Huneus et al. (2011) compared 15 global dust aerosol models that participate
96 the AeroCom model intercomparison project phase I (<http://nansen.ipsl.jussieu.fr/AEROCOM/>)
97 with surface and satellite observations. An eight-fold difference was found in the present-day
98 global dust emissions in the models, ranging from 514 to 4313 Tg yr⁻¹. The model differences in
99 simulated dust burden and optical depth differ by a factor of four and five. The multi-model mean
100 global dust AOD (DAOD) from the AeroCom models is 0.023, lower than an observationally
101 constrained estimate of 0.030±0.005 (1σ) (Ridley et al., 2016). A few global modeling studies
102 (Albani et al., 2014; Kok et al., 2014; Scanza et al., 2015) predict higher DAOD (0.03~0.033) in
103 better agreement with the observations, mainly due to improved dust emission parameterizations
104 and more representative SW refractive indices. But large uncertainties still exist in the CMIP6-
105 type simulations of global dust cycles (A. Zhao et al., 2021), compared with satellite observations
106 (Wu et al., 2020) or reanalysis products (Kok et al., 2021), even near the major dust source regions
107 (Adebisi & Kok, 2020; Evan et al., 2014; Kim et al., 2014; Wu et al., 2020). For dust properties,
108 which either lack direct observational constraints (e.g., emissions), or depend on model
109 representation of aerosol vertical profiles (e.g., dust surface concentration and deposition), the
110 inter-model spread tend to be greater.

111 Uncertainties associated with modeled dust mass loadings and properties affect the
112 assessment of dust radiative and other climatic effects. The net (SW+LW) direct radiative effect
113 (DRE) of dust ranges from -0.5 to +0.35 W m⁻² in recent literature (Di Biagio et al., 2020; Kok et
114 al., 2017; Li et al., 2021; Scanza et al., 2015), while some earlier studies have reported larger
115 negative estimates (Choobari et al., 2014; Forster et al., 2007; Miller et al., 2006; Woodward,
116 2001). In particular, dust DRE is very sensitive to the dust size distribution in models (C. Zhao et
117 al., 2013). Kok et al. (2017) showed that the global DRE of dust is about a factor 2 less cooling
118 than previous estimates (decreasing from -0.46 to -0.20 W m⁻² in their estimate), when the size-
119 resolved dust loadings are constrained by emitted dust size distribution and lifetime. Di Biagio et
120 al. (2020) found that the inclusion of giant particles (≥20 μm) in models could have further
121 weakened the dust cooling effect. Compared to the direct effect, the indirect effects of dust as ice
122 nuclei or cloud condensation nuclei are less understood (DeMott et al., 2010). Dust perturbation
123 on the cloud glaciation processes is not well understood and parameterized with less constraints in
124 large-scale models (DeMott et al., 2015; Fan et al., 2014; Lohmann & Diehl, 2006).

125 Biogeochemical effects associated with uncertainties in dust iron deposition input to ocean
126 biogeochemistry models vary by one order of magnitude among the CMIP5 models (Tagliabue et
127 al., 2016). Moreover, the ESM-simulated iron deposition fluxes may be an order of magnitude
128 smaller than what the more detail iron processing models suggest (Hamilton et al., 2022).

129 The present study evaluates the global life cycle and direct radiative effects of dust
130 simulated by the U.S. DOE Energy Exascale Earth System Model version 1 (E3SMv1) (Golaz et
131 al., 2019). E3SMv1 was built upon CESM1.0 (Neale et al., 2012) with significant improvements
132 in the atmospheric physics and new ocean and sea ice models. It is generally used at a higher
133 vertical and horizontal resolution compared to CESM1.0. The atmospheric component of the
134 E3SMv1 (EAMv1) (Rasch et al., 2019; Xie et al., 2018) uses a higher vertical resolution (72 layers)
135 than its predecessors, and is often configured in the horizontal globally at $\sim 100\text{km}$ (ne30) as the
136 standard (or low) resolution, or $\sim 25\text{km}$ (ne120) as the high resolution. In comparison, the
137 atmosphere component of CESM1.0, e.g., CAM5, has a coarser default resolution of 2°
138 horizontally and 30 vertical layers (Neale et al., 2012). Increasing model resolution in E3SMv1
139 has had large impacts on clouds and precipitation (Xie et al., 2018). Previous studies have shown
140 strong sensitivity of dust generation to increased horizontal resolution (Ridley et al., 2013). Coarse
141 resolution can lead to underestimation of dust emissions by not resolving smaller scale wind
142 variability (K. Zhang et al., 2016). On the other hand, increasing horizontal resolution also
143 modifies the aerosol long-range transport and atmospheric burden, by better accounting for the
144 spatial inhomogeneity in cloud and precipitation (Ma et al., 2015).

145 None of the previous studies we cited have examined the combined effects of increasing
146 model horizontal grid spacing on global dust life cycle through changes in both emissions and
147 removal, and consequently, the impact on DRE. It is unclear what other dust processes in addition
148 to emission are scale-dependent and need to be calibrated for the ESMs moving into higher- or
149 variable- resolution models. Vertically, increasing the number of model layers has been suggested
150 to improve finer dust vertical features near sources (Teixeira et al., 2016) as well as its
151 intercontinental transport (Eastham & Jacob, 2017), but the effect of increasing vertical model
152 resolution on global dust budget and distributions has not been quantified. In addition, the EAMv1
153 includes a number of updates on aerosol physics (Wang et al., 2020), e.g., aerosol resuspension

154 after the re-evaporation below precipitation/clouds, which may have an impact on the coarse-mode
155 aerosol simulations including dust.

156 The manuscript is organized as follows. Section 2 describes the dust aerosol scheme in the
157 EAMv1, modeling experiments, and observational datasets used for model evaluation. It is
158 followed by the model evaluation against various observations in Section 3 that primarily focus on
159 the results from the low-resolution E3SM model configuration with different dust properties.
160 Section 4 presents the dust simulations and direct radiative effects with both the low and high
161 EAMv1 resolutions, compared with other global models. Model sensitivity to the resolution
162 changes is discussed. Finally, a summary of the main findings is given in Section 5.

163 **2 Methodology**

164 **2.1 Dust and aerosol module**

165 The E3SMv1 is a fully coupled ESM (Golaz et al., 2019). Dust-related processes are
166 represented in EAMv1 and the land model component. Total emission fluxes of dust particles are
167 calculated at each model time step following the wind erosion dust scheme by Zender et al. (2003).
168 It depends on the surface wind speed, soil erodibility and a threshold friction velocity. Only the
169 fraction of calculated emission flux of dust particles with diameter $\leq 10 \mu\text{m}$ is represented and
170 simulated in EAMv1, as the coarser particles are currently assumed to fall onto the ground quickly
171 and thus, not leave the grid cell where they are emitted. Although recent studies suggest that giant
172 dust particles (e.g., $>70 \mu\text{m}$) may travel long distances (Does et al., 2018) and contribute to global
173 dust loadings (Adebiyi & Kok, 2020), mechanisms for such long range transport of coarse dust
174 particles remain poorly understood and it is not accounted for in E3SMv1 in the present study. The
175 EAMv1 aerosol module (Wang et al., 2020) is developed from the four-mode version of the Modal
176 Aerosol Module (MAM4) (Liu et al., 2016). It simulates internally mixed major aerosol
177 compounds (sulfate, black carbon, primary and secondary organic matter, dust, sea salt and marine
178 organic aerosols) in three size modes including Aitken, accumulation, and coarse modes, with an
179 additional primary carbon mode representing freshly emitted black carbon and primary organic
180 matter. In each aerosol size mode, mass concentrations of aerosol compounds and a total number
181 concentration of aerosol mixture are calculated at each model time step and evolve in time. It is
182 worth mentioning that although not included here, an interactive gas-phase chemistry is developed

183 (Tang et al., 2021) and available in EAM version 2, allowing the future coupling of dust aerosols
184 with the gas-phase chemistry.

185 Dust is represented in both the accumulation and coarse aerosol modes following emission.
186 The default EAMv1 uses the aerosol size distribution from Zender et al. (2003) to estimate the
187 fractional dust emission fluxes within the (0.1-10) μm size range in diameter (87% of the total
188 emissions) and then distribute the mass between the accumulation (3.2%) and coarse (96.8%)
189 modes, respectively. In this study, we also examine a different dust emission size distribution
190 (Kok, 2011), which predicts more particles in larger sizes, consistent with the recent measurements
191 (Kok et al., 2017). The new size distribution assigns a smaller fraction of the total particle fluxes
192 relative to the default model, about 73% of total mass to the (0.1-10) μm size range. The calculated
193 fractions of the accumulation- and coarse- mode dust mass fluxes further shift the emitted particle
194 size spectra toward larger sizes: about 1.1% in accumulation mode and 98.9% in coarse mode. Dry
195 and wet removal of dust are treated as in CAM5.3 (Liu et al., 2012). A new treatment of aerosol
196 resuspension is used in EAMv1 (Wang et al., 2020) compared to from CAM5.3. The new
197 resuspension parametrization accounts for the release of large-size aerosol particles from
198 evaporated raindrops and then adds them back to the coarse mode. As a result, it increases dry
199 deposition of coarse-mode aerosols that are primarily dust and sea salt aerosols (Wang et al., 2020).

200 Aerosol optical properties are calculated following Ghan and Zaveri (2007) that assumes
201 the volume-mean internally mixed aerosol species. In the released EAMv1, the default SW optical
202 properties of dust are taken from the OPAC package (Hess et al., 1998). In this study we replace
203 them with the observationally based dust optical properties derived from the AERONET
204 measurements (Dubovik et al., 2000). Figure 1 compares the two sets of imaginary dust refractive
205 indices as a function of wavelength. As shown, the AERONET-based imaginary indices are much
206 lower (i.e., less absorbing) than the default sets for dust aerosols, which subsequently affect the
207 calculated dust radiative effects. The LW absorption of mineral dust is treated as in CAM5 (Liu et
208 al., 2012). Aerosol scattering in the LW is neglected in the current model, although this might
209 result in some underestimation of dust LW warming (Dufresne et al., 2002). Dust DRE is
210 calculated as the difference in the instantaneous fluxes at the top of the atmosphere (TOA) between
211 two radiative transfer calculations at each model time step: one with all the aerosol species, and
212 the other with all the aerosol species excluding dust. Both radiation calculations are carried out

213 under the same meteorological conditions (Ghan et al., 2012). The Rapid Radiative Transfer Model
214 for GCM (RRTMG) is used for both SW and LW radiative transfer (Iacono et al., 2008).

215 **2.2 E3SM simulations**

216 Table 1 lists the E3SMv1 model simulations performed. All the simulations employ
217 prescribed sea surface temperature (so called “F-compsets”), and are driven by the IPCC AR5
218 year 2000 anthropogenic aerosols emission inventories representative of the present-day.
219 Specifically,

220 (1) LRes (the control run): represents the last 10-year results of a 11-year free-running
221 simulation with the default EAMv1 configuration ($\sim 1^\circ$ and 72 layers). This is used as the
222 EAMv1 control run for examining the global dust cycle and direct radiative effects
223 compared with other global models and the sensitivity experiments with EAMv1;

224 (2) LResT: is similar to (1), and uses the different dust size distribution and SW absorption
225 properties described above (Letter “T” stands for “This study”). Comparison of (2) with
226 (1) will show the impact of the updated dust properties on the simulated dust distribution
227 and DRE;

228 (3) LResT-Ndg: is similar to (2). Rather than in a free-running mode, this run is nudged to the
229 ECMWF reanalysis temperature and wind for 2009 and 2010 (“Ndg” stands for
230 “Nudging”). The 2010 results were analyzed. Comparison of (3) and (2) will show the
231 impact of nudging to the reanalysis meteorology, in particular, on spatial and temporal
232 correlations with the surface observations;

233 (4) LResT-Ndg-HRtuned: is similar to (3), configured with the high-resolution tuning
234 parameters for atmospheric physics (Caldwell et al., 2019), in which some of the
235 parameters relevant to cloud and convection are re-tuned to achieve TOA global radiative
236 energy budget balance and improve cloud and precipitation simulations (“HRtuned” stands
237 for “High-Resolution tuned”). Comparison of (3) and (4) can inform how does the high-
238 resolution parameter tuning affect the low- and high- resolution E3SM simulations of dust;

239 (5) HRes (High Resolution): is a 5-year run of the high-resolution E3SMv1 ($\sim 0.25^\circ$ and 72
240 layers) and the last 4 years were used for analysis. This HRes simulation uses the same
241 atmospheric physics package as in the default high-resolution E3SMv1 (Caldwell et al.,

2019). Here, more output fields are saved for understanding the dust processes sensitive to resolution in comparison with (1) LRes. Given limited computational resources, we performed 5-year HRes simulations, and used the last 4 years to compare with the LRes simulations for the same time period (years 2-5). There might be noise in some model-predicted mean states that are affected by slow processes such as in the stratosphere, but the main use of this sensitivity study is to compare DAOD, dust vertical distribution in the troposphere, and deposition fluxes at surface between the low and high resolutions. These fields are all related to fast physics, e.g., as shown in Section 4, the global dust lifetime is ~ 2 days and at the regional scale, the lifetime is < 50 days over most of the domain. Therefore, the 4-year averages are sufficient to show the correspondence of these dust fields and the processes related to the resolution changes;

(6) LResZ30: is the last 5-year averages of a 6-year free-running simulation configured with the low horizontal grid spacing ($\sim 1^\circ$) same as (1) LRes, using a coarser vertical resolution of total 30 vertical layers. Similar to (5), the 5-year averages from LResZ30 are reasonable to compare with the years 2-6 results from (1) LRes for understanding the model sensitivity to the vertical resolution change;

(7) LResT-HRtuned: is a 2-year calculation of dust DRE with the low-resolution configuration same as (2) LResT, using the high-resolution tuning parameters. This sensitivity experiment is used to compare with (8), the high-resolution simulation below, for examining the sensitivity of dust DRE to the increase of horizontal resolution while excluding the influences from the high-resolution parameter tuning;

(8) HResT: is similar to (7) with the high-resolution configuration ($\sim 0.25^\circ$ and 72 layers). The DRE calculations require more computational resources especially for the high resolution, so we performed a 2-year simulation with HResT. The last-year results from the 2-year simulations were analyzed for both (7) and (8). Although there might be noise due to interannual variability in the calculated DREs, we limit discussions to the differences between the two resolutions, both of which are under the same influences and driven by those fast processes responding to the resolution changes discussed in (5). The global DAOD in (7) and (8) is tuned slightly higher at 0.04 than LResT at 0.03 to obtain a global

271 AOD ~ 0.14 similar to the observations, while the DAOD is still within the observationally
272 based estimate of 0.03 ± 0.01 (Kok et al., 2017).

273 Since there are no direct constraints of global dust emissions from observations, the annual
274 and global mean DAOD in all the model simulations with E3SMv1 is constrained to 0.026~0.04
275 (Tables 1), approximately matching the observationally based estimate of 0.03 ± 0.01 (Kok et al.,
276 2017), by tuning the emission parameter, i.e., the global scaling factor. As a result, global dust
277 emissions and deposition fluxes are adjusted to a similar level in each set of the sensitivity
278 simulations, independent of model resolution or model physics. We discuss the impact of this
279 emission tuning approach on the simulated dust distributions and DRE in Section 4.

280 **2.3 Observational Datasets**

281 Evaluation of dust life cycle focuses on the DAOD and absorption AOD (AAOD), vertical
282 profiles, and deposition fluxes: the first three are key properties for calculating the DRE, while
283 deposition fluxes are linked to the role of dust as nutrient supply to remote terrestrial and ocean
284 ecosystems. In this study, AOD and AAOD observations are taken from the AERONET Level 1.5
285 daily data products between 2006 and 2015 based on the Version 3 Direct Sun and Inversion
286 Algorithms (Dubovik & King, 2000; Dubovik et al., 2000). Monthly mean AOD is calculated from
287 the daily data for sites with measurements for more than 10 days per month. The yearly means of
288 AOD are then calculated from the monthly averages for sites with more than 10 months of data
289 per year and averaged over the 10-year period (2006-2015) to compare with the model simulations.
290 In addition, a total of 19 ‘dusty’ AERONET sites listed in Table 2 are identified by selecting the
291 sites over land which have a multi-year mean Ångstrom Exponent (AE) < 0.8 . Using this criterion,
292 the simulated dust AOD at all the selected sites except for Trelew in South America contributes
293 more than 50% of the total AOD, suggesting that these sites are heavily influenced by dust
294 aerosols; therefore, the model-observation comparison of total AOD and AAOD at these locations
295 are indicative of the model performance in simulating dust.

296 The CALIOP (Cloud-Aerosol Lidar with Orthogonal Polarization) V4 Aerosol Profiles
297 between 2009 – 2012 are used to evaluate the model dust vertical profiles. Seasonal mean aerosol
298 extinction profiles (Mm^{-1}) are calculated from the CALIOP nighttime product covering most of
299 the source and downwind regions of the Sahara Desert (latitude: 19°S to 49°N, and longitude:
300 97.5°W to 57.5°E) from June to August (JJA) and December to February (DJF). Dust particles are

301 largely coarse sized and non-spherical in shape, resulting in a much larger depolarization ratio than
302 other aerosol types. Speciated dust extinction profiles are thus derived based on the CALIOP
303 depolarization measurements (Yu, Chin, Bian, et al., 2015; Yu et al., 2019). The obtained dust
304 extinction profiles are averaged between 0° and 30°N and for JJA and DJF. These profiles are then
305 used to evaluate the seasonal and long-distance transport of dust and vertical distributions
306 simulated by E3SM.

307 Observations of dust deposition fluxes for the modern climate were estimated from the
308 global data set compiled by Albani et al. (2014) which combined multiple observational sources
309 such as ice core, marine sediments, and terrestrial deposits to provide a global distribution of
310 climatological annual mean dust deposition fluxes. The uncertainty associated with this deposition
311 flux data is discussed in Albani et al. (2014). At the minimum, it provides observational constraints
312 of the geographical pattern and regional variability in dust deposition fluxes.

313 **3 Model Evaluation**

314 This section focuses primarily on the behavior of the low-resolution standard configuration
315 with different choices of model physics (LRes, LResT, LResT-Ndg, and LResT-Ndg-HRtuned).
316 Sensitivity to the model resolution is discussed in Section 4.

317 **3.1 AOD and AAOD**

318 All the E3SMv1 low-resolution simulations yield a similar global DAOD about 0.026-
319 0.029. At the regional scale, Figure 2a shows that the control run LRes predicts the highest DAODs
320 (>0.5) over the major dust source regions including Sahara, Arabian Peninsula, the Gobi and
321 Taklimakan deserts in Asia, and the Australian deserts. Over the remote oceans and within the
322 high latitudes, the modeled DAOD generally falls into the 0.005 to 0.01 range, except for plumes
323 downwind of major dust sources where higher predictions of DAOD close to 0.1 are obtained.
324 Also shown in Fig. 2a, dust aerosols are more prevalent in the Northern Hemisphere than in the
325 Southern Hemisphere in terms of both source strengths and long-distance transport potential.

326 Although global DAOD is similar among the model variants, the dust distributions are
327 different and sensitive to the model dust properties and meteorological conditions. Fig. 2b shows
328 that LResT produces higher DAODs than LRes over some of the dust source regions such as E
329 Asia and Australia and lower predications in the downwind and remote regions. This is because

330 LResT uses a size distribution predicting more coarse particles upon emission (Kok, 2011) that
331 leads to more dry deposition near the sources and thus less aerosol transport over long distances.
332 On the other hand, emissions are increased, under the global DAOD constraint, to compensate for
333 the enhanced deposition that result in higher DAODs near the sources with LResT. Therefore,
334 LResT attributes a larger fraction (85%) of the global DAOD to the coarse-mode particles
335 (diameter > 1 μ m) than LRes (66%). Regionally, this pattern is more evident (Fig. 2c and 2d) that
336 the coarse-mode dusts in LResT dominate the simulated DAOD over 60% in most of the dust-
337 influenced regions even far away from the sources. For the same DAOD, since coarse-mode dust
338 particles result in larger LW warming and less SW cooling than the fine particles, this change of
339 dust size distribution would lead a less cooling net effect of dust in LResT (Di Biagio et al., 2020;
340 Kok et al., 2017).

341 The predicted spatial distribution of DAOD is also sensitive to the model meteorology.
342 Forced by the ERA reanalysis data, LResT-Ndg in Fig. 2e shows weaker long transport of dust
343 indicated by the lower DAOD values in the remote regions compared with LResT in Fig. 2b, due
344 to the enhanced removal. Regional DAODs are also affected by the modified dust emissions, for
345 example, the high-latitude DAOD associated with the Antarctic dust in LResT is not simulated by
346 LResT-Ndg, because the surface (10-meter) windspeeds from the reanalyses in year 2010 used by
347 LResT-Ndg are lower than the model-simulated winds for dust mobilization in Antarctic (Fig. S1
348 and Fig. S2). We will further examine the impact of nudged meteorology on simulated dust spatial
349 distributions in comparison with the AERONET observations below. The high-resolution
350 parameter tuning could also potentially affect the dust simulations through changing the simulated
351 meteorological conditions. As shown in Fig. 2f, compared to LResT-Ndg, LResT-Ndg-HRtuned
352 simulates slightly weaker dust transport, thus smaller DAODs over the remote oceans. It also
353 affects the DAOD distribution by modulating dust mobilization, e.g., over Antarctic (Fig. S1),
354 through the impact on dry convective eddies over land from the high-resolution parameter tuning
355 that may change the surface wind variability. This sensitivity experiment shows that differences
356 in dust simulations between the E3SM low- and high- res simulations (i.e., LRes and HRes in

357 Section 4) may be also attributable to the tuning parameters, although the contribution is small
358 (Fig. S3) except for a few spots.

359 The simulated annual mean AOD and AAOD over the selected dusty sites are compared
360 with the AERONET observations in Figure 3. Table 2 lists the site-specific information and
361 calculated mean statistics. Since most of these dusty sites are located over or near the major source
362 regions in the northern hemisphere (denoted by gray solid circles in Fig. 2a), the annual averages
363 of the site-specific AERONET AOD are high: above 0.4 in the low latitudes ($<15^{\circ}\text{N}$) and above
364 0.15 in the subtropics ($<30^{\circ}\text{N}$). Most of these high AOD values from AERONET are captured in
365 LRes, with a multi-site mean AOD of 0.34 and a spatial correlation coefficient of 0.77. Like LRes,
366 simulations of LResT and LResT-Ndg also generate similar annual mean AODs (0.34 and 0.33,
367 respectively) and a strong spatial correlation with the AERONET AODs (correlation coefficients
368 >0.7). This indicates that the DAOD changes resulting from different dust emission size
369 distributions in LResT and LResT-Ndg reflect primarily on the long-distance transport potential
370 of dust rather than changing the dust concentration over the source regions (Fig. 2). On the other
371 hand, LResT and LResT-Ndg improve the AAOD predictions relative to LRes remarkably in
372 comparison with the AERONET data, as shown in Fig. 3b. The simulated AAOD is reduced by a
373 factor of two at nearly all the sites except for Trelew, where the E3SMv1 predicts very little dust
374 ($<2\%$ of total AOD) probably due to the model low-biased soil erodibility, and thus AAOD is
375 insensitive to the updated dust SW optics in LResT and LResT-Ndg. On average, the mean AAOD
376 over the 19 AERONET sites decreases from 0.038 in LRes to 0.023 and 0.022 in LResT and
377 LResT-Ndg, respectively, showing a great improvement compared with the AERONET mean at
378 0.017. Like AOD, the observed spatial variability in AAOD is also reproduced largely by LRes,
379 LResT and LResT-Ndg with correlation coefficients > 0.7 . Between LResT and LResT-Ndg,
380 nudging to the ERA reanalyse meteorology for a single year (2010) by LResT-Ndg results in a
381 weaker spatial correlation with the AERONET multi-year climatology than LResT, which
382 represents the model-simulated climatology averaged over 10 years. It implies that the free-
383 running E3SMv1 configuration simulates the spatial variability in meteorology that drives dust
384 distributions near the sources reasonably well, but may overestimate the strength that leads to the

385 high-biased AOD (by $\sim+13\%$) and AAOD (by $\sim+35\%$) values compared with the AERONET
386 multi-year means.

387 In addition to the yearly averages, seasonal variations of AOD simulated by LRes, LResT
388 and LResT-Ndg are evaluated in Figure 4 for the 18 dusty sites (excluding the Trelew site where
389 E3SM predicts a low dust concentration). Because the E3SMv1 uses a fixed soil erodibility map,
390 seasonality in the calculated AOD is mainly driven by variations in the meteorological conditions
391 that govern the emissions, transport, and residence time of dust in the atmosphere, such as surface
392 winds, convection intensity, and precipitation. The monthly predictions of AOD by LRes and
393 LResT in the free running configuration correlate reasonably well with the AERONET
394 observations for representing the seasonality of dust loadings near the sources with the calculated
395 correlation coefficients > 0.5 for 14 and 13 out of the 18 sites, respectively. Most of the 13 or 14
396 sites are located within the sub-tropical Northern Hemisphere between 15°N - 30°N . In contrast, the
397 calculated temporal correlations are relatively weaker at lower or higher latitudes; especially for
398 the two low-latitude sites (IER_Cinzana and Banizoumbou), both LRes and LResT yield very low
399 correlation coefficients (0.21~0.33). When nudged towards the ERA reanalysis meteorology in
400 2010, the simulated monthly variability in AOD at these two low-latitude sites improve
401 considerably with LResT-Ndg, as the temporal correlation coefficients with AERONET increase
402 by more than a factor of two (0.75 and 0.69); on the other hand, LResT-Ndg nudging to the single-
403 year reanalyses (year 2010) does not outperform the climatology simulated by LRes or LResT at
404 other sites systematically. This indicates that large uncertainty in the temporal variations of the
405 lower-latitude dust in E3SMv1 are associated with the model representation of the large-scale
406 meteorology in those regions. On the seasonal scale, both the observations and model results yield
407 the yearly maximum AOD near the sources approximately during the hemispheric summer, e.g.,
408 June-July-August (JJA), and shifting to an earlier peak in spring toward the equator, e.g., March-
409 April-May (MAM), while the dust-influenced AODs are consistently the lowest during the
410 hemispheric winter.

411 **3.2 Vertical Distribution**

412 In addition to the column integrated AOD and AAOD, vertical distribution of dust is an
413 important property in the calculation of dust direct radiative effects, in particular for LW radiation
414 flux. Figure 5 compares dust extinction profiles between 0° and 30°N derived from CALIOP and

415 three model experiments (LRes, LResT, and LResT-Ndg) for winter (DJF) and summer (JJA)
416 months, respectively. The CALIOP dust extinctions at 532nm are derived from lidar backscatter
417 signals and particulate depolarization ratios, which are intrinsically different from the bottom-up
418 model calculations based on the dust mass loadings and mass extinction efficiency. The differences
419 between the two approaches may lead to ambiguity in the direct comparison of dust extinction.
420 For instance, in Figure 5b, the large extinction retrievals from CALIOP ($30\sim 40 \text{ Mm}^{-1}$) between
421 60°W to 80°W in the marine boundary layer might be subject to some retrieval uncertainties, such
422 as cloud contamination, and the presence of non-spherical dry sea salt, which are not included in
423 the model-simulated dust extinctions. Thus, the analysis below focuses more on comparing the
424 vertical structure of dust distributions rather than absolute values.

425 The CALIOP extinctions show that the source-region dusts associated with strong
426 convection ascend from the ground up to ~ 6 km in summer, which is about 2 km higher than during
427 winter. All the E3SMv1 simulations capture such seasonal variations in the elevated dust layers,
428 but underpredict the dust extinctions, especially in the free troposphere. These model low biases
429 are greater in summer than in winter when dust is concentrated mostly in the lower troposphere ($<$
430 $3\text{-}4$ km). As a result of the underestimated vertical transport, E3SMv1 also predicts weaker long-
431 range transport of dust westward from the African continent to the tropical/subtropical Atlantic
432 Ocean, compared to the satellite observations (Fig. 5). This indicates that both the vertical transport
433 and removal efficiency of dust in E3SMv1 may need to be re-calibrated to allow more efficient
434 transport of dust in the long distances, as recent studies of aerosol dry deposition indicate that most
435 aerosol models likely overpredict the particle removal compared with the new measurements
436 (Emerson et al., 2020). With more coarser particles emitted, dust extinctions from LResT agree
437 better with the CALIOP retrievals than LRes in the lower troposphere ($< 2\text{ km}$) near the sources,
438 e.g., between 20°W - 20°E . But the underestimation in dust transport is more substantial in LResT
439 as coarser particles fall onto the ground more rapidly.

440 Over the major dust sources, both LRes and LResT in free-running configuration captures
441 the high dust extinctions around 20°E , but underestimate the peak values around the 0° longitude
442 revealed in the observations, especially in JJA. It is likely due to the model bias in underpredicting
443 the surface winds for dust generation in those areas, as when nudged to the reanalysis meteorology,
444 LResT-Ndg simulates higher dust extinctions near the surface and agrees better with the satellite

445 observations between 15°W and 0° in JJA. However, similar to the AOD comparison, LRes and
446 LResT represent the multi-year averaged observations of dust extinction cross sections over the
447 major sources between 0 and 30°N reasonably well, better than LResT-Ndg over a large spatial
448 context.

449 **3.3 Deposition**

450 Dust deposition is a major supplier of the micronutrient iron from the atmosphere to the
451 open ocean (Hamilton et al., 2022; Mahowald et al., 2009). It is thus important to quantify the
452 uncertainty in dust deposition simulated in ESMs (Myriokefalitakis et al., 2018; Tagliabue et al.,
453 2016). Figure 6 shows the global distribution of annual dust deposition fluxes predicted by LRes
454 and LResT, along with a comparison with 108 climatology observations of dust deposition
455 (LResT-Ndg is not shown here since it is nudged to the year 2010 meteorology not representative
456 for comparison with the climatology data). The observational data taken from Albani et al. (2014)
457 are overlaid and denoted by the solid circle symbols with the same color scale used for the model
458 results in Fig. 6a and 6b. In general, large dust particles deposit quickly to the ground after emission
459 through gravitational settling, yielding large deposition fluxes in the vicinity of the major dust
460 source regions, such as the Saharan-Arabian region, deserts in Asia and Australia, and Patagonia.
461 Compared to LRes, LResT predicts lower deposition fluxes over the remote North Pacific and
462 North Atlantic Ocean, because of the reduced dust long-range transport associated with the coarser
463 size distribution, while enhanced deposition is predicted downwind of the Australian dust sources
464 over the South Pacific Ocean from increased emissions near the source regions. Since the dust
465 deposition fluxes are calculated proportional to dust concentrations, the impact of different model
466 configurations on spatial distribution of dust deposition fluxes is similar to DAOD as discussed
467 for Fig. 2.

468 Fig. 6c compares the modeled deposition fluxes with the observations over the 108
469 locations. Most of the model results are within a factor of 10 with the observations, consistent
470 with other global dust studies (Albani et al., 2014; Hamilton et al., 2019). The agreement between
471 the model and data is slightly better over the dust-laden regions, indicated by less scatter and fewer
472 outliers for the observed deposition fluxes larger than $1 \text{ g m}^{-2} \text{ yr}^{-1}$. The regional mean differences
473 between the model predictions and observations are summarized in Table 3. For the locations near
474 the dust sources, such as N. Africa/subtropical NE Atlantic and Asia/Arabian Sea, LRes and LResT

475 overestimate dust deposition by about a factor of 2. The high biases in these two source regions
476 dominate the overall mean bias, although the deposition fluxes are underestimated over the remote
477 oceans, including the North and South Pacific Ocean by about 40-60% and South Atlantic by about
478 20-30%. In the Arctic and Antarctic regions, the observed dust deposition is very low, where the
479 model results have the highest relative biases, which are associated with the high-latitude dust
480 emissions (i.e, in Antarctic) as well as the mid-latitude dust transport. However, the observational
481 data in high latitudes are derived from measurements with great uncertainty, e.g., from ice core,
482 especially for quantifying the present-day dust deposition fluxes. Over all the regions, simulations
483 of LRes and LResT show similar biases (Table 3), either high or low, indicating that the updated
484 dust emission size distributions in LResT do not help much in resolving the model-observation
485 discrepancies in the deposition fluxes. Other factors that could promote transport of dust to the
486 remote regions, for example via revisions to aerosol dry and wet deposition efficiency as well as
487 particle sphericity in calculating settling velocity, may be worth further investigation.

488 **4. Results**

489 **4.1 Global Budgets and Impact of Increased Model Resolution**

490 Table 4 compares the global budgets of dust predicted by E3SMv1 with other modeling
491 studies. For the three low-resolution simulations (LRes, LResT, and LResT-Ndg), dust emissions
492 range from about 4700 to 5400 Tg/yr, higher than CAM5 and other global models listed in Table
493 4, although the observations do not provide a strong constraint on global dust emissions and
494 deposition. Among the different E3SM configurations, LResT and LResT-Ndg require higher dust
495 emissions than the default LRes, because they predict more coarse-mode dust that deposits rapidly
496 to produce a similar AOD, thus requiring more particles emitted to retain the dust loading in the
497 atmosphere. This is more consistent with a recent study (Kok et al., 2021), which estimates a global
498 emission flux of dust greater than current models, approximately 5000 Tg/yr, since it accounts for
499 more coarser dust particles with diameter up to 20 μm . The size differences also lead to higher
500 dust burdens in LResT and LResT-Ndg than in LRes, because coarse-mode dust scatters the
501 sunlight less efficiently than fine-mode dusts and higher dust loadings are needed for matching the

502 DAOD constraint. On the other hand, the global dust burden simulated by LRes is similar to
503 CAM5, which uses the same dust size partitioning upon emission.

504 Dry (or wet) deposition rate (or loss frequency), defined as the ratio of dust dry (or wet)
505 deposition flux (Tg/yr) divided by its mass burden (Tg) in unit of day^{-1} , is often used to quantify
506 the model-simulated dry (or wet) deposition efficiency, rather than absolute deposition fluxes,
507 since the former is not sensitive to the resolution-dependent dust emissions. In the low-resolution
508 E3SMv1 (LRes, LResT and LResT-Ndg), dust dry deposition rate is more than 3 fold greater than
509 the wet deposition rate, indicating that globally, the removal of dust occurs preferentially through
510 dry deposition than wet deposition for their large particle size and low hygroscopicity. Despite
511 different absolute deposition fluxes, three low-resolution E3SMv1 configurations simulate similar
512 dry and wet deposition rates for dust aerosols. Dust lifetime, which is equivalent to the inverse of
513 the total deposition rate, is also loosely dependent on the model dust properties (i.e., size
514 distribution), within 1.7-1.9 days for LRes, LResT and LResT-Ndg. This estimated lifetime is
515 shorter than the typical range of CAM5 (2.6 days) and the AeroCom modeling studies ($4.14 \pm 43\%$
516 days), mainly driven by the larger dust dry deposition rate of E3SM, which is about a factor of two
517 higher. The wet deposition rate of E3SM is similar to CAM5 slightly overestimated compared to
518 other modeling studies (Liu et al., 2012). The predicted strength of dust deposition especially
519 through the dry removal and the short lifetime imply that the low resolution E3SMv1 likely
520 underestimates the vertical transport of dust to the free troposphere. This is consistent with the
521 comparison of the E3SM-simulated extinction profiles with the satellite observations in Section
522 3.2.

523 Without tuning the dust emission parameters, increasing the model horizontal resolution
524 by a factor of 4 from the E3SMv1 low resolution ($\sim 100\text{km}$) to the higher resolution ($\sim 25\text{km}$)
525 simulation results in about a 29% increase of global dust emission fluxes from 4702 to 6044 Tg
526 yr^{-1} , and the global DAOD is increased by 42% from 0.026 to 0.037. This is essentially due to the
527 non-linear strong dependence of dust emissions on the resolved small-scale surface winds (Ridley
528 et al., 2013; K. Zhang et al., 2016). In particular, DAOD shows a stronger dependency on the
529 resolution than emissions, indicated by a larger percent increase. The additional DAOD increase
530 is a result of the weakened dry removal (especially turbulent deposition) of dust at higher
531 horizontal resolution, although there is also a small enhancement in wet removal from the better-

532 resolved clouds and precipitation (Ma et al., 2015). The strong sensitivity to resolution exhibited
533 in the global DAOD suggests that both dust emission and deposition parameterizations are highly
534 resolution- or scale- dependent. In the standard E3SMv1 high-resolution configuration (HRes),
535 dust emissions are adjusted to match the global DAOD constraint of 0.03. After the adjustment,
536 HRes simulates the global dust emissions and DAOD similar to LRes, but the finer horizontal
537 resolution of HRes leads to a ~17% lower dry deposition rate and slightly higher wet deposition
538 rate. As a result, the dust lifetime in the HRes simulation increases to 2.1 days, more comparable
539 to other models than LRes at 1.85 days.

540 In addition to the increased horizontal resolution, the standard E3SMv1 also has a finer
541 vertical resolution with 72 layers compared to its CAM5 predecessor with 30 layers. To examine
542 the effect of increasing the number of vertical layers, one E3SMv1 simulation (LResZ30) was
543 conducted with the same 30 vertical layers as CAM5 (Liu et al., 2012). Constrained by the same
544 global DAOD, LResZ30 generates higher dust emissions than CAM5 for higher horizontal grid
545 spacing, but to a lesser extent compared to LRes. The primary factor determining this difference
546 from LRes is the lower dry deposition rate of dust simulated by LResZ30, which decreases to 0.29
547 day^{-1} by 33% from 0.43 day^{-1} in LRes. The reduction of dust dry deposition also leads to a longer
548 dust lifetime at 2.4 days. This sensitivity model experiment of decreasing the E3SMv1 vertical
549 resolution reveals similar effects on the simulated dust burden and lifetime to the model refinement
550 of horizontal resolution, although the underlying mechanisms may be different. For example, both
551 gravitational settling and turbulent deposition responsible for dust dry removal are influenced
552 equally by changing the vertical resolution, while increasing horizontal resolution has a larger
553 impact on the latter, resulting in a larger contribution of gravitational settling of dust in total dry
554 deposition (from 75% in LRes to 78% in HRes). In contrast to dry deposition, refining the model
555 resolution, either horizontally or vertically, has moderate effects on the dust wet deposition rate
556 globally, although it could be more significant on the regional scales and for hygroscopic aerosol
557 species such as sea salt or sulfate aerosols (Caldwell et al., 2019).

558 The comparison of global dust budgets with different E3SMv1 configurations suggests that
559 the global mean DAOD does not fully constrain the life cycle of dust. When constrained by the
560 same DAOD, the model diversity in global emissions, deposition, burden, and lifetime of dust
561 between E3SM configurations and other models are evident, as summarized in Table 4. These
562 model disagreements imply a wide range of differences in dust transport and spatial distributions

563 that could further influence the direct and indirect radiative effects of dust. Therefore, it is
564 important to understand the contributing processes to the inter-model differences in dust global
565 budgets and the manifested impact. Sensitivity of the dust simulations to dust emission size
566 distribution and SW optics (between LRes and LResT) has been discussed in Section 3 compared
567 with the observations. Here we further examine the impact of increased model resolution both
568 horizontally and vertically on individual dust processes.

569 **4.2 Effects of Increasing Resolution on DAOD**

570 Figure 7 shows the global distributions of annual mean DAOD, emissions, and lifetime
571 simulated by HRes, and their differences from LRes. HRes simulates the geographical pattern and
572 hemispheric contrast of annual DAOD similar to LRes (Fig. 2a), however, there are great
573 differences in their regional DAOD values; as shown in in Fig. 7b, the DAOD differences between
574 the two simulations vary by region in both sign and magnitude. HRes generally predicts higher
575 DAODs over the major dust source regions (>25%) than LRes as well as the adjacent oceans
576 downwind of the dust transport. In particular, over the Arabian Peninsula, Middle East, and
577 Taklimakan desert in E Asia, the DAOD predictions in HRes are more than doubled relative to
578 LRes. These regional increases of DAOD are compensated by lower predictions over the western
579 Sahel, tropical/subtropic Atlantic, S. America and Europe, adding up to a similar global mean
580 DAOD between HRes and LRes. Such large positive or negative changes in DAOD ($>\pm 0.1$) could
581 potentially affect the simulated regional radiation balance and hydrological cycle. They are driven
582 by the compound effects of changes in dust emissions and deposition rate.

583 The HRes simulation of dust emissions and the differences from LRes are illustrated in
584 Fig. 7c and 7d. Emission fluxes in the dust source regions generally increase with higher model
585 horizontal resolution as expected for HRes, leading to larger local DAODs. However, some HRes
586 grid cells are associated with lower dust emission fluxes than LRes, e.g., negative changes over
587 North Africa, which contribute to the smaller DAOD in HRes over Europe and the southeastern
588 Atlantic. The decrease of dust emissions from LRes to HRes is due to a larger global scaling factor
589 used in HRes to scale the total emissions down to the LRes level; in those grid cells, the increase
590 of emissions due to the resolved surface winds are smaller than the decrease of emissions resulting
591 from the global scaling. These regionally different responses in dust emissions, resulting from the
592 empirical global tuning approach, would alter the relative contributions of dust from the various

593 sources. For example, dust emissions from the Middle East and E Asia will constitute a larger
594 fraction in the global emission fluxes in HRes than in LRes because of its increased dust
595 mobilization, while the North African dust emissions decrease. Subsequently, it would change the
596 spatial distributions of simulated dust loadings, DAOD, and radiative effects, because dust
597 transport is influenced by the regional meteorology and dust properties such as size and mineral
598 composition are source-dependent.

599 In addition to the emissions, global distributions of dust burden and DAOD are also
600 influenced by the dry or wet removal (deposition) processes represented in LRes and HRes. To
601 understand the resolution effect on deposition, dust lifetime (day), which is the inverse of
602 deposition rate (day^{-1}) and insensitive to the column dust burden, simulated by HRes and the
603 changes from LRes are shown in Fig. 7e and Fig. 7f, respectively. Although the globally averaged
604 dust lifetime is short ~ 2 -4 days, dust deposits much slower outside the source regions after being
605 lifted into the free troposphere, e.g., longer than 10 days over the subtropical oceans and in the
606 high latitudes. In comparison, it is less than 1-2 days over the source regions or in the tropical
607 precipitating regions and mid-latitude frontal systems where wet removal is efficient. Refining the
608 horizontal grid spacing may lead to shorter dust lifetime, because of the higher surface windspeed
609 that increases friction velocity, thus causing larger dry deposition velocity at the surface (L. Zhang
610 et al., 2001). In addition, dust dry deposition rate in the column also depends on the vertical
611 transport of dust particles, which is enhanced within HRes (discussed below in Section 4.2). Since
612 the free-troposphere dust is removed by sedimentation only, slower than the boundary-layer dust,
613 the enhanced vertical transport will thus lead to longer dust lifetime. This effect generally
614 dominates the increased surface dry deposition velocity over the convective dust source regions,
615 resulting in longer dust lifetime in those regions (Fig. 7f), such as in North Africa for more than
616 0.5 day ($\sim +50\%$). On the other hand, dust wet deposition is enhanced in HRes due to resolved
617 cloud and precipitation fields, decreasing the local lifetime of the transported dust, e.g., over the
618 subtropical southeasten Atlantic and northeastern Pacific. Longer (shorter) dust lifetime
619 contributes to a larger (smaller) dust burden, therefore, enhanced (reduced) DAOD in those
620 regions, but also the net changes in DAOD also depend on the modified emissions that determine
621 the amount of dust mobilized and emitted to the atmosphere.

622 Opposing to the effect of the horizontal refinement (Fig. 7b), increasing the number of
623 vertical layers from 30 in LResZ30 to 72 in LRes leads to the reduction of DAOD over most of

624 the dust-influenced regions as shown in Fig. 8a, except for a few downwind regions. These changes
625 in DAOD also cannot be explained solely by the emission changes in Fig. 8b, as LRes with finer
626 vertical resolution produces different profiles of stability and turbulence, which in fact causes
627 higher surface winds, thus stronger dust mobilization over most of the erodible surfaces, e.g., the
628 western North Africa, where the DAOD changes, however, are primarily negative. As discussed
629 above, the higher surface winds in LRes also enhance the surface deposition velocity, thus
630 reducing the residence time of dust over the source regions (Fig. 8c). Therefore, LRes predicts less
631 elevated dust to the free troposphere and advected in long distances than LResZ30 (discussed
632 below in Section 4.3), thus smaller DAODs near the source regions, e.g., for the North African
633 dust plumes over the equatorial Atlantic Ocean and South America. The weakened wet removal in
634 LRes relative to LResZ30 increases the local lifetime of the transported dust over most of the
635 remote oceans, which may or may not lead to larger DAOD values depending also on the changes
636 of local dust burden from transport.

637 It is worth noting that the ambient atmospheric conditions especially relative humidity, to
638 which DAOD is sensitive, could also be influenced by the resolution changes (both horizontally
639 and vertically) through the dust climate feedback in the free-running model simulations. It is
640 considered to be secondary though, compared to the direct changes in dust aerosol fields discussed
641 here.

642 **4.3 Effects of Increasing Resolution on Vertical Distribution**

643 In addition to the column integrated DAOD, dust vertical distribution is also sensitive to
644 the model resolution as shown in Figure 9. LRes predicts the weakest vertical transport of dust
645 around the major dust sources in both hemispheres, i.e., 15°N, followed by 40°N and 25°S,
646 consistent with the shortest dust lifetime (Table 4). Compared to LRes, both HRes (with higher
647 horizontal resolution) and LResZ30 (with lower vertical resolution) simulate enhanced uplift of
648 dust to the upper troposphere, leading to greater global burdens. Thus, model refinement in the
649 horizontal (from LRes to HRes) has the opposing effects on dust vertical distribution compared to
650 refining the vertical resolution (from LResZ30 to LRes). The main difference between them is that
651 the vertical transport of dust in HRes with increased horizontal resolution is enhanced, as a result
652 of resolved convective or nonconvective (e.g., orographic) ascent and stronger turbulent mixing in
653 the boundary layer (indicated by a smaller contribution from the turbulent deposition in dry

654 removal), while a weaker upward transport of dust is simulated by LRes with increased vertical
655 resolution, because of the enhanced dust dry deposition at the surface associated with stronger
656 surface winds. Although HRes also predicts higher surface winds thus larger surface deposition,
657 this effect on dust vertical distribution is weaker over the source regions thus dominated by the
658 enhancement of vertical motion that enables stronger vertical transport of dust particles in HRes.
659 The strong sensitivity of dust vertical distribution to the varying model resolution through
660 interactions with surface winds and boundary-layer dynamics clearly demonstrates that the model
661 representations of the surface dry deposition, sedimentation and vertical transport processes of
662 dust are highly scale-dependent, besides the dust emission parameterization.

663 While LResZ30 does not change the zonal-mean maximum dust source locations from
664 LRes, i.e., still center around the 15°N latitudes, HRes shows the increased relative strength of
665 dust loadings around 40°N as well as 30°N and 25°S, because the emissions in those regions have
666 a stronger dependency on resolved surface winds than those areas near 15°N. The enhanced dust
667 vertical transport around 40°N in HRes further leads to the stronger poleward transport in the upper
668 troposphere above 500 hPa. Because of the low mass extinction coefficient and low hygroscopicity
669 of dust aerosols especially in the free troposphere, these model discrepancies in dust vertical
670 mixing ratios do not make substantial differences in DAOD, e.g., in the high latitudes (<0.01 , Fig.
671 7b). Therefore, the dust vertical distribution is not well constrained by the column integrated
672 DAOD, in particular the global mean DAOD. The elevated dust, on the other hand, could act as
673 highly-active ice nucleation particles in mixed or ice phase clouds causing changes to indirect
674 radiative effects. It is critical to constrain the vertical transport of dust into the free troposphere.

675 **4.4 Effects of Increasing Resolution on Deposition Fluxes**

676 As a key input to the ocean biogeochemistry, it is important to examine the sensitivity of
677 the absolute dust deposition fluxes to model resolution in line with the development of the high-
678 resolution coupled ESMs. The differences in the simulated dust deposition fluxes between
679 different resolution configurations are shown in Fig. 10. Since the dust deposition fluxes
680 corresponds to the emissions, HRes simulates larger deposition fluxes than LRes over most of the
681 domain, except for the areas influenced by the lowered emissions or with enhanced removal. In
682 particular, over the major high-nutrient low-chlorophyll biological regions in the sub-Arctic
683 Pacific and Southern Ocean, dust deposition fluxes are increased by $>25\%$ in HRes, suggesting an

684 enhanced nutrient supply to the ocean biogeochemistry if coupled with a higher-resolution
685 atmospheric model. Additionally, the HRes model also predicts more than 2-fold annual dust
686 deposition into the Arctic region than LRes, which could have important implications on the
687 acceleration of ice/snow melting in the high latitudes by lowering the surface albedo. In contrast,
688 the impact of higher vertical resolution is opposing to the horizontal refinement. Compared to
689 LResZ30, LRes predicts larger deposition fluxes over the major dust sources including Antarctic
690 (Fig. 8c), but underestimates in most of the other regions, except for a few regions with higher
691 DAOD (thus larger burden) due to increased lifetime (Fig. 8c). These differences in the changes
692 of dust deposition fluxes with higher horizontal or vertical resolution correspond largely to the
693 DAOD changes (dust burden changes), which in turn depend on the combined effects on various
694 dust processes discussed in Section 4.2.

695 Compared with the observational data in Fig. 6c and Table 3, the model underestimation
696 in the remote oceans such as N. Pacific is reduced with HRes, since it predicts larger deposition
697 fluxes than LRes over most of the domain. But the overestimation in the absolute dust deposition
698 fluxes over the dust-laden regions such as N. Africa and the adjacent subtropical Atlantic is
699 enlarged by HRes, except for Antarctic, where the model high bias is substantially reduced (i.e.,
700 by a factor of 4 in the Table 3) due to the lowered Antarctic dust emissions (Fig. 7d). Contrary to
701 the HRes-induced changes, the LRes simulations of dust deposition agree better with the
702 observations than LResZ30 over the main dust deposition oceans near the sources but are even
703 more underestimated in the remote oceans. As shown in the Table 3 and Fig. 6c, the resolution
704 effects on deposition fluxes have a larger impact in the remote regions, whereas near the sources,
705 dust deposition fluxes are influenced more by the model representation of dust properties, e.g.,
706 particle size, sphericity, or deposition velocity, which either the low or high resolution E3SMv1
707 simulations are high-biased.

708 **4.5 Dust Direct Radiative Effects**

709 Figure 11 shows the calculated DRE of dust at TOA with the different E3SMv1
710 configurations. LRes, which is the default E3SMv1 configuration, predicts positive DREs of dust
711 over the major source regions such as Sahara, Arabian Peninsula and Central Asia, exceeding 10
712 Wm^{-2} , due to the light absorption of dust minerals when located over the highly reflective surfaces.
713 Also, moderately positive DREs of dust are estimated over the mid-latitude oceans likely above

714 the storm tracks and snow- or ice-covered surface in high latitudes, while negative DREs are found
715 in the lower latitudes over oceans or land associated with relatively dark surfaces. Overall, the
716 mean dust DRE by LRes gives a slightly negative global forcing of -0.08 Wm^{-2} at TOA. Using the
717 less-absorbing imaginary indices inferred from the AERONET measurements, LResT predicts
718 more negative DREs over most of the domain, mainly because of the reduced dust SW absorption
719 (AAOD). The globally averaged net DRE of dust decreases to -0.42 Wm^{-2} , which is more negative
720 about a factor of five higher in magnitude than LRes. The model-calculated global energy budgets
721 in the column: at the TOA, in the atmosphere and at surface, are summarized in Table 5. About
722 2/3 of the reduction in the TOA DRE estimated by LResT relative to LRes is due to the lower
723 atmospheric absorption in SW (about 50% less), which is consistent with the AAOD reduction
724 (Section 3.1). Additionally, LResT also predicts more boundary-layer dusts and less vertical and
725 horizontal transport than LRes in comparison with CALIPSO (Section 3.2), which further
726 contributes to the more negative DREs in SW, as the boundary-layer dusts are less likely to be
727 lifted above the clouds with a brighter underlying surface. For the LW DRE, LResT increases
728 slightly from $+0.08 \text{ Wm}^{-2}$ in LRes to 0.1 Wm^{-2} , as shown in Table 5, due to the increased LW
729 warming of coarse-mode dust (Kok et al., 2017). Therefore, the net DRE differences between
730 LResT and LRes are primarily attributable to the SW DRE changes.

731 The impact of increasing horizontal resolution on dust DRE is illustrated in Figure 11c for
732 differences between HResT and LResT_HRtuned (same as LResT but using the high-resolution
733 tuning parameters). Therefore, differences in the estimated dust DRE between HResT and
734 LResT_HRtuned are attributable to the resolution effect on dust simulations solely, i.e., not
735 affected by the different physics tuning parameters. Both simulations are performed with the
736 updated dust size distribution and optical properties as in LResT that are planned for the next
737 version of E3SM, i.e., E3SMv2. They are also tuned to the same global DAOD of about
738 $0.038\sim 0.04$, which is slightly higher than LResT (in order to get a HResT AOD close to the satellite
739 estimate of 0.14) but still within the uncertainty of the observational estimate (0.03 ± 0.01). As
740 shown in Fig. 11c, higher horizontal resolution leads to regionally dependent changes in the
741 predicted dust DREs. The geographical pattern of the DRE differences between HResT and
742 LResT_HRtuned corresponds approximately to the DAOD changes between HRes and LRes in
743 Fig. 7b. Specifically, higher DAODs with the finer-resolution simulations (HResT or HRes) result
744 in stronger dust DREs, either more positively or negatively, relative to the coarse-resolution

745 simulations (LResT or LRes). For instance, the strength of the positive DREs of dust over the
746 Sahara Desert and Arabian Peninsula would be enhanced by increasing horizontal resolution, as
747 well as the negative effects in most of the Asia (Fig. 7b). On the other hand, because of the
748 decreased DAODs, the negative DREs of dust downwind of the North African sources across the
749 Atlantic Ocean and over the South America would be weakened with higher resolution. In addition
750 to DAOD, the resolution effect on dust vertical distribution also affects the strength of dust DREs.
751 More dusts particles can loft at the higher resolution, leading to the weakening (positive changes)
752 of the negative DREs over Central Asia (Fig. 9b), despite the increased DAOD. Since the LW
753 DRE of dust increases with height, it is enhanced globally by $+0.02 \text{ Wm}^{-2}$ (14%) in HResT (Table
754 5), comparable to the effect of changing the dust size distribution. The impact of increasing
755 resolution on the globally averaged dust net DRE is small with a slightly weaker negative effect
756 due to the enhanced LW warming, although the regional changes are greater and different in sign.

757 The comparison of the estimated dust DREs with other modeling studies is shown in Figure
758 12 for the SW, LW and net effects, respectively. In order to reduce the influences from different
759 DAODs, the DRE estimates from HResT are scaled to a global DAOD of 0.029 same as the E3SM
760 low resolution runs (LRes and LResT), and denoted as HResT* in Fig. 12 and Table 5. The default
761 E3SMv1 model (LRes) predicts a small dust net DRE with a negative value of -0.08 Wm^{-2} at TOA,
762 which is more positive than -0.17 Wm^{-2} from CAM5 (Scanza et al., 2015), -0.45 Wm^{-2} by the
763 AeroCom models taken from Kok et al. (2017) and an observationally constrained estimate of -
764 0.2 Wm^{-2} (Kok et al., 2017), primarily due to the weaker SW cooling (smaller negative SW DRE).
765 After updating the dust SW absorption and size-segregated emissions, E3SMv1 at both low and
766 high resolutions (LResT and HResT*) estimates a more negative net DRE of about -0.42 Wm^{-2} ,
767 which is within the AeroCom model estimates (-0.3 to -0.6 Wm^{-2}), although both the SW and LW
768 effects are relatively lower. Kok et al. (2017) suggested that the fine-size bias in the AeroCom
769 models probably contributed to their larger SW cooling. Indeed, the updated E3SM with the size
770 correction that shifts more emitted dust particles from the accumulation mode toward larger sizes
771 ($\text{diameter} \leq 10 \mu\text{m}$) predicts a SW DRE of $\sim -0.5 \text{ Wm}^{-2}$, and agrees better with CAM5 (Scanza et
772 al., 2015) and the observationally constrained estimate (Kok et al., 2017). Kok et al. (2017) also
773 includes coarser particles with $10 \mu\text{m} \leq \text{diameter} \leq 20 \mu\text{m}$ and a recent study by Di Biagio et al.
774 (2020) shows that even coarser particles with $\text{diameter} \geq 20 \mu\text{m}$ should be considered in global
775 models. These very coarse particles would further reduce the contribution by smaller (cooling)

776 particles to the global dust cycle, as Di Biagio et al. (2020) obtains a smaller negative DRE in SW
777 (-0.25 Wm^{-2}), about half of the other model calculations.

778 Dust particle size is also one of the large sources of uncertainty for the LW effect. The size
779 correction implemented to E3SM and higher horizontal resolution increases the LW warming
780 effect by 50% from $+0.08$ to $+0.01$ and $+0.12 \text{ Wm}^{-2}$ progressively, but it is still lower than other
781 studies ranging from $+0.17$ to $+0.25 \text{ Wm}^{-2}$ as shown in Fig. 12. Inclusion of the coarser particles
782 (diameter $\geq 10 \mu\text{m}$) to E3SMv1 would directly increase the estimated dust LW effect, e.g., Kok et
783 al. (2017) indicates that the coarse dust particles (i.e., $10 \mu\text{m} \leq \text{diameter} \leq 20 \mu\text{m}$) could produce an
784 additional positive DRE of 0.03 Wm^{-2} (0.01 to 0.06) globally. The uncertainty in LW DRE may
785 also stem from the dust refractive indices, as E3SMv1 neglects the regional variability in dust LW
786 optics (Di Biagio et al., 2017), e.g., which changes their DRE LW estimates between $+0.09$ and
787 $+0.36 \text{ Wm}^{-2}$. Another uncertainty is from the LW scattering that is not considered in E3SMv1 but
788 by other studies such as Kok et al. (2017). In addition, the LW effect is very sensitive to the dust
789 layer height, which is one of the least constrained dust properties in models compared with the
790 observations, and could potentially cause great inter-modal differences. As discussed in Section
791 4.3, the higher horizontal and vertical resolution of E3SMv1 have a large impact on the dust
792 vertical distribution that may contribute to the differences in LW DRE.

793 To exclude the uncertainty in DAOD, the DRE efficiency, defined as the DRE produced
794 per unit of global DAOD, is calculated. For E3SMv1, it ranges from 3.5 (LResT) to 4 Wm^{-2}
795 (HResT) in LW, both of which are lower than those of CAM5 (5.2 Wm^{-2}) and the observational
796 estimate (8.3 Wm^{-2}). For the SW DRE efficiency, E3SMv1 generates the largest negative values
797 from -17.9 (LResT) to -18.3 Wm^{-2} (HResT) compared to the $-10. \text{ Wm}^{-2}$ by CAM5 and -16.7 Wm^{-2}
798 2 constrained by the observations. Similar to the direct comparison of DRE, the consistently low
799 (or high) differences in LW (or SW) DRE efficiencies estimated by E3SMv1 indicate that the
800 globally averaged dust size in this global model might still be too small assuming the
801 observationally constrained estimates provide the correct ranges with high-quality datasets.
802 Including coarser dust particles would generate larger LW warming and smaller SW cooling that

803 could nudge the calculated DRE efficiencies toward the observational estimates. Other
804 uncertainties as mentioned above might also help to explain the differences.

805 **5. Discussion and Conclusions**

806 Quantification of dust life cycle and radiative effects in ESMs has important implications
807 for improving the model's capabilities for water cycle and biogeochemistry studies in response to
808 climate change. Unlike anthropogenic aerosols, dust aerosols not only influence the climate system
809 as an external forcer but also account for a significant fraction of the direct climate feedback
810 associated with all aerosols (Kok et al., 2018). Because the dust simulation is sensitive to the model
811 representation of meteorological and climate states, dust simulations are often subject to great
812 uncertainties, as indicated by a wide diversity in simulated dust quantities among models and
813 between models and observations (Huneeus et al., 2011; A. Zhao et al., 2021). These uncertainties,
814 most of which are unconstrained, further affect the assessment of dust radiative and climate effects.
815 As part of development of the DOE E3SM on exascale computing platforms, this study examines
816 the simulated global life cycle and direct radiative effects of dust in the recently released E3SMv1,
817 resulting from model physics improvements and increased model resolution.

818 Our study shows that the default E3SMv1 constrained by the global DAOD simulates the
819 geographical pattern and seasonal variations in DAOD reasonably well, compared with the
820 AERONET surface measurements. On the other hand, it overestimates the dust aerosol absorption
821 in SW by a factor of two, which leads to a more positive net DRE (-0.08 Wm^{-2}) than its precedent
822 model CAM5 (-0.17 Wm^{-2}). By switching to the less absorbing dust refractive indices as well as
823 an emission size distribution with more coarse particles emitted, the dust SW cooling simulated
824 by E3SMv1 is increased and is closer to the observationally based estimate by Kok et al. (2017).
825 For dust vertical distribution, E3SMv1 captures seasonal variations of the elevated dust layers over
826 the major source regions, but underpredicts the dust extinctions compared with the CALIOP data,
827 especially in the upper troposphere. The low biases in the model simulations are greater in summer
828 than winter. As a result of the underestimation of vertical transport, E3SMv1 also predicts a weaker
829 long-range transport of dust compared with the satellite observations and a shorter dust lifetime
830 (~ 2 days) than most of other models. The simulated deposition fluxes are underestimated in remote

831 oceans, but the global dust deposition is dominated by the high biases near the sources over the
832 main dust deposition regions, compared with the climatology data composite.

833 The impact of increasing model resolution on dust simulations was examined with
834 E3SMv1. It is critical to understand what individual dust processes are scale- or resolution-
835 dependent and the subsequent impact on the dust radiative effects and deposition fluxes for
836 implications on future development of high-resolution ESMs such as the Simple Cloud-Resolving
837 E3SM Atmospheric Model (SCREAM) (Caldwell et al., 2021) or regionally refined variable
838 resolution ESMs (Tang et al., 2019). This study finds that in addition to the emission fluxes, dust
839 removal, especially dry deposition rate, is highly scale-dependent, which in turn affects the dust
840 lifetime, atmospheric burden and DAOD. Specifically, increasing horizontal resolution (from
841 100km to 25km) without tuning results in a larger enhancement in global DAOD (+42%) than seen
842 in the emissions themselves (+29%), because it is combined with a reduction of dry deposition
843 rate (-21%) and increase of lifetime. With the global tuning of DAOD (through dust emissions), it
844 still leads to a decreased dry deposition rate by -17%. In contrast, refinement of vertical resolution
845 (from 30 to 72 layers) increases the dust dry deposition rate (+45%), thus resulting in a shorter
846 lifetime, opposing to the horizontal effect. The global wet removal of dust is relatively less
847 sensitive to the increased model resolution both horizontally and vertically.

848 Furthermore, we showed that the uniform scaling of dust emission factor to constrain global
849 DAOD does not eliminate the remarkable and nonuniform changes of DAOD on the regional
850 scales, due to the compound resolution effects on dust emissions, removal, and vertical transport.
851 Dust vertical distributions and deposition fluxes are also highly sensitive to the resolution changes,
852 and these quantities are not well constrained by the column integrated DAOD, in particular the
853 global mean. As the elevated dusts in the free troposphere are a major source of ice nucleation
854 particles for mixed- and ice- phase clouds and the nutrient-enriching dust deposition is vital for
855 terrestrial and ocean ecosystems, better observational constraints of dust vertical distribution and
856 deposition fluxes are needed for representing the dust indirect radiative and biogeochemical effects
857 in the future ESMs with higher resolution.

858 The global DAOD constraint does effectively curb the impact of increasing horizontal
859 resolution on the global mean dust net DRE. Compared to the low-resolution configuration of
860 E3SMv1, the high-resolution configuration by 4 times in the horizontal estimates a slightly weaker

861 negative dust DRE by about 4% (+0.03 Wm⁻²). However, the large regional differences in DAOD
862 and vertical distributions with higher model resolution can lead to positive or negative direct
863 perturbations on the energy balance ranging from -9 to +4 Wm⁻² on the annual mean basis, which
864 is sufficient to potentially affect the regional hydrological cycle. The updated dust optics and
865 emission size distribution lead to improved dust SW and net DREs of -0.52 Wm⁻² and -0.42 Wm⁻²
866 than the default E3SMv1, compared with the observationally based estimates of -0.5 (-0.85 to -
867 0.15 Wm⁻²) and -0.2 (-0.48 to +0.2 Wm⁻²). But even with the corrected fine-size bias in dust
868 particles upon emission, the calculated SW and LW DRE efficiencies by E3SM still indicate that
869 the globally averaged dust size might still be too small, compared with the observations, showing
870 a stronger SW cooling and weaker LW warming. This finding about the atmospheric presence of
871 possibly more coarser dust particles is consistent with some recent global model studies (Di Biagio
872 et al., 2020; Kok et al., 2017). Other uncertainties such as the dust LW scattering (Dufresne et al.,
873 2002), refractive indices (Di Biagio et al., 2017), mineral speciation (Li et al., 2021), and particle
874 sphericity (Hamilton et al., 2020) could also contribute to the inter-modal differences in dust DRE.

875 It is challenging to constrain the simulated dust life cycle with multiple observational
876 variables, amid uncertainties in the datasets. In E3SMv1, the evaluation of dust DRE suggests that
877 the abundance of coarse particles may be underrepresented in all model configuration, but simply
878 shifting particles upon emission or in transport toward large sizes would aggravate the high biases
879 in the simulated dust deposition fluxes near the sources and low biases in remote oceans. To
880 harmonize these uncertainties, further investigation into constraining processes affecting long
881 range transport and improving dust dry deposition and convective transport to the upper
882 atmosphere is warranted. Furthermore, this study demonstrates the strong sensitivity of model
883 representation of dust processes beyond emissions (such as dry deposition and vertical transport)
884 to both horizontal and vertical model resolution, and the impact on direct radiative effects of dust.
885 It also adds a cautionary note to the use of global dust AOD at 550nm as the only constraint for

886 dust simulations, highlighting the need of developing observational constraints for dust size, LW
 887 optical properties and vertical profiles as well as variability in deposition fluxes.

888

889 **Acknowledgments**

890 This research was supported as part of the Energy Exascale Earth System Model (E3SM) project,
 891 funded by the U.S. Department of Energy (DOE), Office of Science, Office of Biological and
 892 Environmental Research (BER). The authors thank all the E3SM project team members for their
 893 efforts in developing and supporting the E3SM. YF would like to acknowledge the support of
 894 Argonne National Laboratory (ANL) provided by the U.S. DOE Office of Science, under
 895 Contract No. DE-AC02-06CH11357. The Pacific Northwest National Laboratory (PNNL) is
 896 operated for U.S. DOE by Battelle Memorial Institute under contract DE-AC05-76RL01830. The
 897 work at Lawrence Livermore National Laboratory (LLNL) was performed under the auspices of
 898 the U.S. DOE by Lawrence Livermore National Laboratory under Contract DE-AC52-
 899 07NA27344. The work at Brookhaven National Laboratory (BNL) was supported by the U.S.
 900 DOE Office of Science under contract DE-SC0012704. DSH and NMM would like to
 901 acknowledge support from DOE DE-SC0021302. HY was supported by NASA
 902 CALIPSO/CloudSat Science Team project administered by David Considine. Simulations and
 903 analysis were performed by using the computing cluster (Anvil) supported by the BER Earth
 904 System Modeling program and operated by the Laboratory Computing Resource Center (LCRC)
 905 at ANL, as well as the computational resources at the National Energy Research Scientific
 906 Computing Center (NERSC), a DOE Office of Science User Facility supported by the Office of
 907 Science of the U.S. Department of Energy under contract DE-AC02-05CH11231.

908 **Code and Data Availability**

909 The E3SM project, code, simulation configurations, model output, and tools to work with the
 910 output are described at the website (<https://e3sm.org>). The E3SMv1 model has been released and
 911 made available through the GitHub repository (<https://github.com/E3SM-Project/E3SM>). Model
 912 output data are accessible directly on NERSC.

913

914 **References**

- 915
 916 Adebisi, A. A., & Kok, J. F. (2020). Climate models miss most of the coarse dust in the atmosphere. *Science*
 917 *Advances*, 6(15), eaaz9507. <https://www.science.org/doi/abs/10.1126/sciadv.aaz9507>
 918 Albani, S., Mahowald, N. M., Perry, A. T., Scanza, R. A., Zender, C. S., Heavens, N. G., et al. (2014). Improved
 919 dust representation in the Community Atmosphere Model. *Journal of Advances in Modeling Earth Systems*,
 920 6(3), 541-570. <Go to ISI>://WOS:000344387900004
 921 Amiri-Farahani, A., Allen, R. J., Neubauer, D., & Lohmann, U. (2017). Impact of Saharan dust on North Atlantic
 922 marine stratocumulus clouds: importance of the semidirect effect. *Atmospheric Chemistry and Physics*,
 923 17(10), 6305-6322. <Go to ISI>://WOS:000401923600001
 924 Caldwell, P. M., Mamejtanov, A., Tang, Q., Van Roekel, L. P., Golaz, J. C., Lin, W. Y., et al. (2019). The DOE
 925 E3SM Coupled Model Version 1: Description and Results at High Resolution. *Journal of Advances in*
 926 *Modeling Earth Systems*. <Go to ISI>://WOS:000502308300001

- 927 Caldwell, P. M., Terai, C. R., Hillman, B., Keen, N. D., Bogenschutz, P., Lin, W., et al. (2021). Convection-
 928 Permitting Simulations with the E3SM Global Atmosphere Model. *Journal of Advances in Modeling Earth*
 929 *Systems*, n/a(n/a), e2021MS002544. <https://doi.org/10.1029/2021MS002544>.
 930 <https://doi.org/10.1029/2021MS002544>
- 931 Choobari, O. A., Zawar-Reza, P., & Sturman, A. (2014). The global distribution of mineral dust and its impacts on
 932 the climate system: A review. *Atmospheric Research*, 138, 152-165. <Go to
 933 ISI>://WOS:000333504300012
- 934 DeMott, P. J., Prenni, A. J., Liu, X., Kreidenweis, S. M., Petters, M. D., Twohy, C. H., et al. (2010). Predicting
 935 global atmospheric ice nuclei distributions and their impacts on climate. *Proceedings of the National*
 936 *Academy of Sciences of the United States of America*, 107(25), 11217-11222. <Go to
 937 ISI>://WOS:000279058000014
- 938 DeMott, P. J., Prenni, A. J., McMeeking, G. R., Sullivan, R. C., Petters, M. D., Tobo, Y., et al. (2015). Integrating
 939 laboratory and field data to quantify the immersion freezing ice nucleation activity of mineral dust
 940 particles. *Atmospheric Chemistry and Physics*, 15(1), 393-409. <Go to ISI>://WOS:000347958200023
- 941 DeMott, P. J., Sassen, K., Poellot, M. R., Baumgardner, D., Rogers, D. C., Brooks, S. D., et al. (2003). African dust
 942 aerosols as atmospheric ice nuclei. *Geophysical Research Letters*, 30(14). <Go to
 943 ISI>://WOS:000184599400002
- 944 Dentener, F. J., Carmichael, G. R., Zhang, Y., Lelieveld, J., & Crutzen, P. J. (1996). Role of mineral aerosol as a
 945 reactive surface in the global troposphere. *Journal of Geophysical Research-Atmospheres*, 101(D17),
 946 22869-22889. <Go to ISI>://WOS:A1996VN18400012
- 947 Di Biagio, C., Balkanski, Y., Albani, S., Boucher, O., & Formenti, P. (2020). Direct Radiative Effect by Mineral
 948 Dust Aerosols Constrained by New Microphysical and Spectral Optical Data. *Geophysical Research*
 949 *Letters*, 47(2), e2019GL086186. <https://agupubs.onlinelibrary.wiley.com/doi/abs/10.1029/2019GL086186>
- 950 Di Biagio, C., Formenti, P., Balkanski, Y., Caponi, L., Cazaunau, M., Pangu, E., et al. (2017). Global scale
 951 variability of the mineral dust long-wave refractive index: a new dataset of in situ measurements for
 952 climate modeling and remote sensing. *Atmos. Chem. Phys.*, 17(3), 1901-1929.
 953 <https://acp.copernicus.org/articles/17/1901/2017/>
- 954 Does, M. v. d., Knippertz, P., Zschenderlein, P., Harrison, R. G., & Stuut, J.-B. W. (2018). The mysterious long-
 955 range transport of giant mineral dust particles. *Science Advances*, 4(12), eaau2768.
 956 <https://www.science.org/doi/abs/10.1126/sciadv.aau2768>
- 957 Doherty, O. M., & Evan, A. T. (2014). Identification of a new dust-stratocumulus indirect effect over the tropical
 958 North Atlantic. *Geophysical Research Letters*, 41(19), 6935-6942. <Go to ISI>://WOS:000344913800052
- 959 Dubovik, O., & King, M. D. (2000). A flexible inversion algorithm for retrieval of aerosol optical properties from
 960 Sun and sky radiance measurements. *Journal of Geophysical Research-Atmospheres*, 105(D16), 20673-
 961 20696. <Go to ISI>://WOS:000089107600017
- 962 Dubovik, O., Smirnov, A., Holben, B. N., King, M. D., Kaufman, Y. J., Eck, T. F., & Slutsker, I. (2000). Accuracy
 963 assessments of aerosol optical properties retrieved from Aerosol Robotic Network (AERONET) Sun and
 964 sky radiance measurements. *Journal of Geophysical Research-Atmospheres*, 105(D8), 9791-9806. <Go to
 965 ISI>://WOS:000086658600004
- 966 Dufresne, J. L., Gautier, C., Ricchiazzi, P., & Fouquart, Y. (2002). Longwave scattering effects of mineral aerosols.
 967 *Journal of the Atmospheric Sciences*, 59(12), 1959-1966. <Go to ISI>://WOS:000175533700003
- 968 Eastham, S. D., & Jacob, D. J. (2017). Limits on the ability of global Eulerian models to resolve intercontinental
 969 transport of chemical plumes. *Atmospheric Chemistry and Physics*, 17(4), 2543-2553. <Go to
 970 ISI>://WOS:000395136300001
- 971 Emerson, E. W., Hodshire, A. L., DeBolt, H. M., Bilsback, K. R., Pierce, J. R., McMeeking, G. R., & Farmer, D. K.
 972 (2020). Revisiting particle dry deposition and its role in radiative effect estimates. *Proceedings of the*
 973 *National Academy of Sciences*, 117(42), 26076. <http://www.pnas.org/content/117/42/26076.abstract>
- 974 Evan, A. T., Flamant, C., Fiedler, S., & Doherty, O. (2014). An analysis of aeolian dust in climate models.
 975 *Geophysical Research Letters*, 41(16), 5996-6001. <Go to ISI>://WOS:000342755400040
- 976 Evan, A. T., Foltz, G. R., Zhang, D. X., & Vimont, D. J. (2011). Influence of African dust on ocean-atmosphere
 977 variability in the tropical Atlantic. *Nature Geoscience*, 4(11), 762-765. <Go to
 978 ISI>://WOS:000296723500013
- 979 Fan, Leung, L. R., DeMott, P. J., Comstock, J. M., Singh, B., Rosenfeld, D., et al. (2014). Aerosol impacts on
 980 California winter clouds and precipitation during CalWater 2011: local pollution versus long-range
 981 transported dust. *Atmos. Chem. Phys.*, 14(1), 81-101. <https://www.atmos-chem-phys.net/14/81/2014/>

- 982 Feng, Y., & Penner, J. E. (2007). Global modeling of nitrate and ammonium: Interaction of aerosols and
 983 tropospheric chemistry. *Journal of Geophysical Research-Atmospheres*, 112(D1). <Go to
 984 ISI>://WOS:000243352300001
- 985 Forster, P., Ramaswamy, V., Artaxo, P., Bernsten, T., Betts, R., Fahey, D. W., et al. (2007). Changes in
 986 Atmospheric Constituents and in Radiative Forcing. In *Climate Change 2007: The Physical Science Basis. Contribution of Working Groups I to the Fourth Assessment Report of the Intergovernmental Panel on
 987 Climate Change*. Cambridge, United Kingdom and New York, NY, USA: Cambridge University Press.
- 988 Ghan, S. J., Liu, X., Easter, R. C., Zaveri, R., Rasch, P. J., Yoon, J. H., & Eaton, B. (2012). Toward a Minimal
 989 Representation of Aerosols in Climate Models: Comparative Decomposition of Aerosol Direct, Semidirect,
 990 and Indirect Radiative Forcing. *Journal of Climate*, 25(19), 6461-6476. <Go to
 991 ISI>://WOS:000309653800001
- 992 Ghan, S. J., & Zaveri, R. A. (2007). Parameterization of optical properties for hydrated internally mixed aerosol.
 993 *Journal of Geophysical Research-Atmospheres*, 112(D10). <Go to ISI>://WOS:000246838800003
- 994 Golaz, J. C., Caldwell, P. M., Van Roekel, L. P., Petersen, M. R., Tang, Q., Wolfe, J. D., et al. (2019). The DOE
 995 E3SM Coupled Model Version 1: Overview and Evaluation at Standard Resolution. *Journal of Advances in
 996 Modeling Earth Systems*, 11(7), 2089-2129. <Go to ISI>://WOS:000480282800012
- 997 Hamilton, D. S., Perron, M. M. G., Bond, T. C., Bowie, A. R., Buchholz, R. R., Guieu, C., et al. (2022). Earth,
 998 Wind, Fire, and Pollution: Aerosol Nutrient Sources and Impacts on Ocean Biogeochemistry. *Annual
 999 Review of Marine Science*, 14(1), null. <https://www.annualreviews.org/doi/abs/10.1146/annurev-marine-031921-013612>
- 1000 Hamilton, D. S., Scanza, R. A., Feng, Y., Guinness, J., Kok, J. F., Li, L. L., et al. (2019). Improved methodologies
 1001 for Earth system modelling of atmospheric soluble iron and observation comparisons using the Mechanism
 1002 of Intermediate complexity for Modelling Iron (MIMI v1.0). *Geoscientific Model Development*, 12(9),
 1003 3835-3862. <Go to ISI>://WOS:000484142100001
- 1004 Hamilton, D. S., Scanza, R. A., Rathod, S. D., Bond, T. C., Kok, J. F., Li, L., et al. (2020). Recent (1980 to 2015)
 1005 Trends and Variability in Daily-to-Interannual Soluble Iron Deposition from Dust, Fire, and Anthropogenic
 1006 Sources. *Geophysical Research Letters*, 47(17), e2020GL089688.
 1007 <https://agupubs.onlinelibrary.wiley.com/doi/abs/10.1029/2020GL089688>
- 1008 Hess, M., Koepke, P., & Schult, I. (1998). Optical properties of aerosols and clouds: The software package OPAC.
 1009 *Bulletin of the American Meteorological Society*, 79(5), 831-844. <Go to ISI>://WOS:000073809200007
- 1010 Huneus, N., Schulz, M., Balkanski, Y., Griesfeller, J., Prospero, J., Kinne, S., et al. (2011). Global dust model
 1011 intercomparison in AeroCom phase I. *Atmospheric Chemistry and Physics*, 11(15), 7781-7816. <Go to
 1012 ISI>://WOS:000293826500024
- 1013 Iacono, M. J., Delamere, J. S., Mlawer, E. J., Shephard, M. W., Clough, S. A., & Collins, W. D. (2008). Radiative
 1014 forcing by long-lived greenhouse gases: Calculations with the AER radiative transfer models. *Journal of
 1015 Geophysical Research-Atmospheres*, 113(D13). <Go to ISI>://WOS:000257431600004
- 1016 Jickells, T. D., An, Z. S., Andersen, K. K., Baker, A. R., Bergametti, G., Brooks, N., et al. (2005). Global iron
 1017 connections between desert dust, ocean biogeochemistry, and climate. *Science*, 308(5718), 67-71. <Go to
 1018 ISI>://WOS:000228221500033
- 1019 Kim, D., Chin, M., Yu, H. B., Diehl, T., Tan, Q., Kahn, R. A., et al. (2014). Sources, sinks, and transatlantic
 1020 transport of North African dust aerosol: A multimodel analysis and comparison with remote sensing data.
 1021 *Journal of Geophysical Research-Atmospheres*, 119(10), 6259-6277. <Go to
 1022 ISI>://WOS:000337766600034
- 1023 Kok, J. F. (2011). Does the size distribution of mineral dust aerosols depend on the wind speed at emission?
 1024 *Atmospheric Chemistry and Physics*, 11(19), 10149-10156. <Go to ISI>://WOS:000296357300009
- 1025 Kok, J. F., Adebisi, A. A., Albani, S., Balkanski, Y., Checa-Garcia, R., Chin, M., et al. (2021). Improved
 1026 representation of the global dust cycle using observational constraints on dust properties and abundance.
 1027 *Atmos. Chem. Phys.*, 21(10), 8127-8167. <https://acp.copernicus.org/articles/21/8127/2021/>
- 1028 Kok, J. F., Mahowald, N. M., Fratini, G., Gillies, J. A., Ishizuka, M., Leys, J. F., et al. (2014). An improved dust
 1029 emission model - Part 1: Model description and comparison against measurements. *Atmospheric Chemistry
 1030 and Physics*, 14(23), 13023-13041. <Go to ISI>://WOS:000346140100026
- 1031 Kok, J. F., Ridley, D. A., Zhou, Q., Miller, R. L., Zhao, C., Heald, C. L., et al. (2017). Smaller desert dust cooling
 1032 effect estimated from analysis of dust size and abundance. *Nature Geoscience*, 10(4), 274-278. <Go to
 1033 ISI>://WOS:000398162800014
- 1034 Kok, J. F., Ward, D. S., Mahowald, N. M., & Evan, A. T. (2018). Global and regional importance of the direct dust-
 1035 climate feedback. *Nature Communications*, 9. <Go to ISI>://WOS:000422649500003

- 1038 Lau, K. M., Kim, K. M., Sud, Y. C., & Walker, G. K. (2009). A GCM study of the response of the atmospheric
 1039 water cycle of West Africa and the Atlantic to Saharan dust radiative forcing. *Annales Geophysicae*,
 1040 27(10), 4023-4037. <Go to ISI>://WOS:000271356500028
- 1041 Li, L., Mahowald, N. M., Miller, R. L., Pérez García-Pando, C., Klose, M., Hamilton, D. S., et al. (2021).
 1042 Quantifying the range of the dust direct radiative effect due to source mineralogy uncertainty. *Atmos.*
 1043 *Chem. Phys.*, 21(5), 3973-4005. <https://acp.copernicus.org/articles/21/3973/2021/>
- 1044 Liu, Easter, R. C., Ghan, S. J., Zaveri, R., Rasch, P., Shi, X., et al. (2012). Toward a minimal representation of
 1045 aerosols in climate models: description and evaluation in the Community Atmosphere Model CAM5.
 1046 *Geoscientific Model Development*, 5(3), 709-739. <Go to ISI>://WOS:000305964700001
- 1047 Liu, Ma, P. L., Wang, H., Tilmes, S., Singh, B., Easter, R. C., et al. (2016). Description and evaluation of a new
 1048 four-mode version of the Modal Aerosol Module (MAM4) within version 5.3 of the Community
 1049 Atmosphere Model. *Geoscientific Model Development*, 9(2), 505-522. <Go to
 1050 ISI>://WOS:000376933700003
- 1051 Liu, C., Chu, B., Liu, Y., Ma, Q., Ma, J., He, H., et al. (2013). Effect of mineral dust on secondary organic aerosol
 1052 yield and aerosol size in α -pinene/NO_x photo-oxidation. *Atmospheric Environment*, 77, 781-789.
 1053 <http://www.sciencedirect.com/science/article/pii/S1352231013004378>
- 1054 Lohmann, U., & Diehl, K. (2006). Sensitivity studies of the importance of dust ice nuclei for the indirect aerosol
 1055 effect on stratiform mixed-phase clouds. *Journal of the Atmospheric Sciences*, 63(3), 968-982. <Go to
 1056 ISI>://WOS:000236735900010
- 1057 Ma, P.-L., Rasch, P. J., Wang, M., Wang, H., Ghan, S. J., Easter, R. C., et al. (2015). How does increasing
 1058 horizontal resolution in a global climate model improve the simulation of aerosol-cloud interactions?
 1059 *Geophysical Research Letters*, 42(12), 2015GL064183. <http://dx.doi.org/10.1002/2015GL064183>
- 1060 Mahowald. (2011). Aerosol Indirect Effect on Biogeochemical Cycles and Climate. *Science*, 334(6057), 794-796.
 1061 <Go to ISI>://WOS:000296849600043
- 1062 Mahowald, Engelstaedter, S., Luo, C., Sealy, A., Artaxo, P., Benitez-Nelson, C., et al. (2009). Atmospheric Iron
 1063 Deposition: Global Distribution, Variability, and Human Perturbations. *Annual Review of Marine Science*,
 1064 1, 245-278. <Go to ISI>://WOS:000267421700011
- 1065 Miller, R. L., Cakmur, R. V., Perlwitz, J., Geogdzhayev, I. V., Ginoux, P., Koch, D., et al. (2006). Mineral dust
 1066 aerosols in the NASA goddard institute for Space Sciences ModelE atmospheric general circulation model.
 1067 *Journal of Geophysical Research-Atmospheres*, 111(D6). <Go to ISI>://WOS:000236730400004
- 1068 Miller, R. L., Tegen, I., & Perlwitz, J. (2004). Surface radiative forcing by soil dust aerosols and the hydrologic
 1069 cycle. *Journal of Geophysical Research-Atmospheres*, 109(D4). <Go to ISI>://WOS:000189373800006
- 1070 Myriokefalitakis, S., Ito, A., Kanakidou, M., Nenes, A., Krol, M. C., Mahowald, N. M., et al. (2018). Reviews and
 1071 syntheses: the GESAMP atmospheric iron deposition model intercomparison study. *Biogeosciences*,
 1072 15(21), 6659-6684. <https://bg.copernicus.org/articles/15/6659/2018/>
- 1073 Neale, R. B., Chen, C.-C., Gettelman, A., Lauritzen, P. H., Park, S., Williamson, D. L., et al. (2012). Description of
 1074 the NCAR Community Atmosphere Model (CAM 5.0). *NCAR/TN-486C STR*.
 1075 http://www.cesm.ucar.edu/models/cesm1.0/cam/docs/description/cam5_desc.pdf
- 1076 Painter, T. H., Skiles, S. M., Deems, J. S., Bryant, A. C., & Landry, C. C. (2012). Dust radiative forcing in snow of
 1077 the Upper Colorado River Basin: 1. A 6 year record of energy balance, radiation, and dust concentrations.
 1078 *Water Resources Research*, 48. <Go to ISI>://WOS:000306905800001
- 1079 Rasch, P. J., Xie, S., Ma, P. L., Lin, W., Wang, H., Tang, Q., et al. (2019). An Overview of the Atmospheric
 1080 Component of the Energy Exascale Earth System Model. *Journal of Advances in Modeling Earth Systems*,
 1081 11(8), 2377-2411. <https://doi.org/10.1029/2019MS001629>. <https://doi.org/10.1029/2019MS001629>
- 1082 Ridley, D. A., Heald, C. L., Kok, J. F., & Zhao, C. (2016). An observationally constrained estimate of global dust
 1083 aerosol optical depth. *Atmospheric Chemistry and Physics*, 16(23), 15097-15117. <Go to
 1084 ISI>://WOS:000389209000005
- 1085 Ridley, D. A., Heald, C. L., Pierce, J. R., & Evans, M. J. (2013). Toward resolution-independent dust emissions in
 1086 global models: Impacts on the seasonal and spatial distribution of dust. *Geophysical Research Letters*,
 1087 40(11), 2873-2877. <Go to ISI>://WOS:000321261600072
- 1088 Rosenfeld, D., Rudich, Y., & Lahav, R. (2001). Desert dust suppressing precipitation: A possible desertification
 1089 feedback loop. *Proceedings of the National Academy of Sciences of the United States of America*, 98(11),
 1090 5975-5980. <Go to ISI>://WOS:000168883700010
- 1091 Scanza, R. A., Mahowald, N., Ghan, S., Zender, C. S., Kok, J. F., Liu, X., et al. (2015). Modeling dust as component
 1092 minerals in the Community Atmosphere Model: development of framework and impact on radiative
 1093 forcing. *Atmospheric Chemistry and Physics*, 15(1), 537-561. <Go to ISI>://WOS:000347958200030

- 1094 Skiles, S. M., Painter, T. H., Deems, J. S., Bryant, A. C., & Landry, C. C. (2012). Dust radiative forcing in snow of
 1095 the Upper Colorado River Basin: 2. Interannual variability in radiative forcing and snowmelt rates. *Water*
 1096 *Resources Research*, 48. <Go to ISI>://WOS:000306905800002
- 1097 Sokolik, I. N., Toon, O. B., & Bergstrom, R. W. (1998). Modeling the radiative characteristics of airborne mineral
 1098 aerosols at infrared wavelengths. *Journal of Geophysical Research-Atmospheres*, 103(D8), 8813-8826.
 1099 <Go to ISI>://WOS:000073290900016
- 1100 Solmon, F., Nair, V. S., & Mallet, M. (2015). Increasing Arabian dust activity and the Indian summer monsoon.
 1101 *Atmospheric Chemistry and Physics*, 15(14), 8051-8064. <Go to ISI>://WOS:000358799000019
- 1102 Tagliabue, A., Aumont, O., DeAth, R., Dunne, J. P., Dutkiewicz, S., Galbraith, E., et al. (2016). How well do global
 1103 ocean biogeochemistry models simulate dissolved iron distributions? *Global Biogeochemical Cycles*, 30(2),
 1104 149-174. <Go to ISI>://WOS:000372963900005
- 1105 Tang, Q., Klein, S. A., Xie, S., Lin, W., Golaz, J. C., Roesler, E. L., et al. (2019). Regionally refined test bed in
 1106 E3SM atmosphere model version 1 (EAMv1) and applications for high-resolution modeling. *Geosci. Model*
 1107 *Dev.*, 12(7), 2679-2706. <https://gmd.copernicus.org/articles/12/2679/2019/>
- 1108 Tang, Q., Prather, M. J., Hsu, J., Ruiz, D. J., Cameron-Smith, P. J., Xie, S., & Golaz, J. C. (2021). Evaluation of the
 1109 interactive stratospheric ozone (O3v2) module in the E3SM version 1 Earth system model. *Geosci. Model*
 1110 *Dev.*, 14(3), 1219-1236. <https://gmd.copernicus.org/articles/14/1219/2021/>
- 1111 Tegen, I., Lacs, A. A., & Fung, I. (1996). The influence on climate forcing of mineral aerosols from disturbed soils.
 1112 *Nature*, 380(6573), 419-422. <Go to ISI>://WOS:A1996UD59000055
- 1113 Teixeira, J. C., Carvalho, A. C., Tuccella, P., Curci, G., & Rocha, A. (2016). WRF-chem sensitivity to vertical
 1114 resolution during a saharan dust event. *Physics and Chemistry of the Earth, Parts A/B/C*, 94, 188-195.
 1115 <http://www.sciencedirect.com/science/article/pii/S1474706515000364>
- 1116 Vinoj, V., Rasch, P. J., Wang, H., Yoon, J.-H., Ma, P.-L., Landu, K., & Singh, B. (2014). Short-term modulation of
 1117 Indian summer monsoon rainfall by West Asian dust. *Nature Geoscience*, 7(4), 308-313.
 1118 <https://doi.org/10.1038/ngeo2107>
- 1119 Wang, H., Easter, R. C., Zhang, R., Ma, P.-L., Singh, B., Zhang, K., et al. (2020). Aerosols in the E3SM Version 1:
 1120 New Developments and Their Impacts on Radiative Forcing. *Journal of Advances in Modeling Earth*
 1121 *Systems*, 12(1), e2019MS001851. <https://agupubs.onlinelibrary.wiley.com/doi/abs/10.1029/2019MS001851>
- 1122 Woodward, S. (2001). Modeling the atmospheric life cycle and radiative impact of mineral dust in the Hadley
 1123 Centre climate model. *Journal of Geophysical Research-Atmospheres*, 106(D16), 18155-18166. <Go to
 1124 ISI>://WOS:000170579400036
- 1125 Wu, M., Liu, X., Yu, H., Wang, H., Shi, Y., Yang, K., et al. (2020). Understanding processes that control dust
 1126 spatial distributions with global climate models and satellite observations. *Atmos. Chem. Phys.*, 20(22),
 1127 13835-13855. <https://acp.copernicus.org/articles/20/13835/2020/>
- 1128 Xie, S. C., Lin, W. Y., Rasch, P. J., Ma, P. L., Neale, R., Larson, V. E., et al. (2018). Understanding Cloud and
 1129 Convective Characteristics in Version 1 of the E3SM Atmosphere Model. *Journal of Advances in Modeling*
 1130 *Earth Systems*, 10(10), 2618-2644. <Go to ISI>://WOS:000450413200013
- 1131 Yu, H., Chin, M., Bian, H. S., Yuan, T. L., Prospero, J. M., Omar, A. H., et al. (2015). Quantification of trans-
 1132 Atlantic dust transport from seven-year (2007-2013) record of CALIPSO lidar measurements. *Remote*
 1133 *Sensing of Environment*, 159, 232-249. <Go to ISI>://WOS:000352749000018
- 1134 Yu, H., Chin, M., Yuan, T. L., Bian, H. S., Remer, L. A., Prospero, J. M., et al. (2015). The fertilizing role of
 1135 African dust in the Amazon rainforest: A first multiyear assessment based on data from Cloud-Aerosol
 1136 Lidar and Infrared Pathfinder Satellite Observations. *Geophysical Research Letters*, 42(6), 1984-1991. <Go
 1137 to ISI>://WOS:000353170000047
- 1138 Yu, H., Tan, Q., Chin, M., Remer, L. A., Kahn, R. A., Bian, H., et al. (2019). Estimates of African Dust Deposition
 1139 Along the Trans-Atlantic Transit Using the Decadelong Record of Aerosol Measurements from CALIOP,
 1140 MODIS, MISR, and IASI. *Journal of Geophysical Research: Atmospheres*, 124(14), 7975-7996.
 1141 <https://doi.org/10.1029/2019JD030574>. <https://doi.org/10.1029/2019JD030574>
- 1142 Zender, C. S., Bian, H. S., & Newman, D. (2003). Mineral Dust Entrainment and Deposition (DEAD) model:
 1143 Description and 1990s dust climatology. *Journal of Geophysical Research-Atmospheres*, 108(D14). <Go to
 1144 ISI>://WOS:000184611000001
- 1145 Zhang, K., Zhao, C., Wan, H., Qian, Y., Easter, R. C., Ghan, S. J., et al. (2016). Quantifying the impact of sub-grid
 1146 surface wind variability on sea salt and dust emissions in CAM5. *Geosci. Model Dev.*, 9(2), 607-632.
 1147 <https://www.geosci-model-dev.net/9/607/2016/>

- 1148 Zhang, L., Gong, S., Padro, J., & Barrie, L. (2001). A size-segregated particle dry deposition scheme for an
 1149 atmospheric aerosol module. *Atmospheric Environment*, 35(3), 549-560.
 1150 <https://www.sciencedirect.com/science/article/pii/S1352231000003265>
- 1151 Zhao, A., Ryder, C. L., & Wilcox, L. J. (2021). How well do the CMIP6 models simulate dust aerosols? *Atmos.*
 1152 *Chem. Phys. Discuss.*, 2021, 1-32. <https://acp.copernicus.org/preprints/acp-2021-578/>
- 1153 Zhao, C., Chen, S., Leung, L. R., Qian, Y., Kok, J. F., Zaveri, R. A., & Huang, J. (2013). Uncertainty in modeling
 1154 dust mass balance and radiative forcing from size parameterization. *Atmos. Chem. Phys.*, 13(21), 10733-
 1155 10753. <https://www.atmos-chem-phys.net/13/10733/2013/>
- 1156 Zhao, C., Liu, X., & Leung, L. R. (2012). Impact of the Desert dust on the summer monsoon system over
 1157 Southwestern North America. *Atmospheric Chemistry and Physics*, 12(8), 3717-3731. <Go to
 1158 ISI>://WOS:000304054800011
- 1159 Zhao, C., Liu, X., Leung, L. R., & Hagos, S. (2011). Radiative impact of mineral dust on monsoon precipitation
 1160 variability over West Africa. *Atmospheric Chemistry and Physics*, 11(5), 1879-1893. <Go to
 1161 ISI>://WOS:000288368900003
- 1162 Zhu, A., Ramanathan, V., Li, F., & Kim, D. (2007). Dust plumes over the Pacific, Indian, and Atlantic oceans:
 1163 Climatology and radiative impact. *Journal of Geophysical Research-Atmospheres*, 112(D16). <Go to
 1164 ISI>://WOS:000249335400002
- 1165
- 1166

Table 1 Description of the E3SMv1 (or EAMv1) model simulations included

#	Simulation	Horizontal resolution	Vertical layers	Results	Physics parameter tuning	Dust size distri.	SW optics	DAOD/AOD	DRE
(1)	LRes (EAMv1)	~1°	72	Years 2-11 (cold start)	FC5AV1C -04P2	Default	Default	0.029/0.142	Yes
Sensitivity experiments to dust properties, nudging and high-resolution parameter tuning									
(2)	LResT	~1°	72	Years 2-11 (cold start)	FC5AV1C -04P2	Kok (2011)	AERO NET	0.029/0.141	Yes
(3)	LResT-Ndg	~1°	72	2010 (nudging, initialized from the 2009 run)	FC5AV1C -04P2	Kok (2011)	AERO NET	0.026/0.135	No
(4)	LResT-Ndg-HRtuned	~1°	72	2010 (nudging, initialized from the 2009 run)	FC5AV1C -H01A	Kok (2011)	AERO NET	0.026/0.129	No
Sensitivity experiments to resolution									
(5)	HRes (EAMv1)	~0.25°	72	Years 2-5 (cold start)	FC5AV1C -H01A	Default	Default	0.032/0.135	No
(6)	LResZ30	~1°	30	Years 2-6 (cold start)	FC5AV1C -04P2	Default	Default	0.029/0.145	No
Resolution effect on direct radiative effect									
(7)	LResT-HRtuned	~1°	72	Year 2 (cold start)	FC5AV1C -H01A	Kok (2011)	AERO NET	0.038/0.149	Yes
(8)	HResT	~0.25°	72	Year 2 (cold start)	FC5AV1C -H01A	Kok (2011)	AERO NET	0.04/0.147	Yes

Table 2 Location of the selected 19 AERONET dusty sites and annual mean AOD and AAOD from the E3SM model (LRes, LResT, and LResT-Ndg) and AERONET (Obs). Also shown are the calculated Pearson’s correlation coefficients between the AERONET (Obs) data and model calculations

Site	Lat.	Lon.	Obs	LRes	LResT	LResT-Ndg	Obs	LRes	LResT	LResT-Ndg
				AOD				AAOD		
Trelew	-43.25	294.69	0.036	0.035	0.036	0.033	0.005	0.002	0.002	0.002
Tinga_Tingana	-28.98	139.99	0.042	0.134	0.138	0.108	0.005	0.014	0.009	0.007
DMN_Maine_Soraa	13.22	12.02	0.466	0.742	0.799	0.768	0.038	0.090	0.054	0.050
IER_Cinzana	13.28	354.07	0.436	0.475	0.467	0.397	0.025	0.051	0.030	0.025
Banizoumbou	13.55	2.67	0.482	0.591	0.600	0.522	0.023	0.067	0.039	0.033
Dakar	14.39	343.04	0.445	0.487	0.467	0.402	0.023	0.052	0.030	0.026
Agoufou	15.35	358.52	0.461	0.493	0.489	0.421	0.022	0.056	0.031	0.026
Hada_El-Sham	21.80	39.73	0.358	0.304	0.290	0.315	0.007	0.034	0.020	0.022
KAUST_Campus	22.30	39.10	0.379	0.313	0.303	0.323	0.015	0.036	0.021	0.023
Tamanrasset_INM	22.79	5.53	0.249	0.284	0.285	0.327	0.014	0.033	0.019	0.021
Masdar_Institute	24.44	54.62	0.369	0.335	0.342	0.312	0.018	0.039	0.024	0.023
Solar_Village	24.91	46.40	0.395	0.271	0.269	0.288	0.024	0.031	0.019	0.021
Karachi	24.95	67.14	0.435	0.295	0.300	0.392	0.030	0.030	0.020	0.026
Dhadnah	25.51	56.32	0.359	0.340	0.351	0.305	0.024	0.040	0.024	0.022
El_Farafra	27.06	27.99	0.191	0.343	0.363	0.352	0.009	0.043	0.026	0.026
Santa_Cruz_Tenerife	28.47	343.75	0.154	0.221	0.206	0.166	0.005	0.017	0.010	0.007
Ouarzazate	30.93	353.09	0.140	0.154	0.153	0.177	0.010	0.016	0.010	0.012
Saada	31.63	351.84	0.206	0.155	0.154	0.166	0.012	0.016	0.010	0.011
Medenine-IRA	33.50	10.64	0.163	0.421	0.467	0.520	0.008	0.052	0.031	0.036
Multi-site mean			0.30	0.34	0.34	0.33	0.017	0.038	0.023	0.022
Correlation: Obs vs				(0.77)	(0.72)	(0.70)		(0.72)	(0.74)	(0.71)

Table 3 Comparisons of dust annual deposition fluxes ($\text{g m}^{-2} \text{yr}^{-1}$) by region. The observational data are taken from Albani et al. (2014). Also shown are the regional mean deposition fluxes from LRes, LResT and HRes as well as the ratios over the observational data (numbers in parentheses)

Region (# of sites)	Observations	LRes	LResT	HRes
N Africa/Sub. Atlantic (27)	12	24.7 (2.1)	32.8 (2.7)	28.4 (2.4)
Europe/N. Atlantic (13)	6.4	5.9 (0.9)	6.5 (1.)	6.41 (1.)
Asia/Arabian Sea (15)	26	38.7 (1.5)	52 (2.0)	51.4 (2.0)
N. America (2)	1.9	1.7 (0.9)	2.3 (1.2)	2.76 (1.5)
N Pacific (15)	2.3	1.15 (0.5)	1.25 (0.5)	1.55 (0.7)
S Atlantic/S. America (6)	7.7	5.3 (0.7)	7.14 (0.9)	6.82 (0.9)
S Pacific/Australia (13)	1.4	0.67 (0.5)	0.86 (0.6)	1.11 (0.8)
Antarctica (15)	0.003	0.06 (19.1)	0.08 (23.9)	0.02 (5.2)
Arctic (2)	0.029	0.07 (2.4)	0.08 (2.6)	0.08 (2.8)
All the sites (108):	8.35	12.8 (1.5)	16.9 (2.0)	15.8 (1.9)

Table 4 Global budgets for dust in E3SMv1 (LRes, LResT, LResT-Ndg, HRes, and LResZ30) compared with CAM5 and other modeling studies

	E3SMv1					CAM5	Other studies
	LRes	LResT	LResT-Ndg	HRes	LResZ30		
Horizontal Res	1°	1°	1°	0.25°	1°	1.9°	Variable
Vertical layers	72	72	72	72	30	30	Variable
Emission (Tg/yr)	4377	5921	5256	4751	4173	3122	1840±49%
Deposition (Tg/yr):							
Dry	3385(0.42)	4657(0.46)	4088(0.41)	3320(0.35)	2948(0.29)	(0.24)	(0.23±84%)
Wet	990(0.12)	1260(0.12)	1160(0.12)	1331(0.14)	1298(0.13)	(0.14)	(0.08±42%)
Burden (Tg)	22.2	27.9	27.1	27.0	28.3	22.4	19.2±40%
Lifetime (day)	1.85	1.72	1.88	2.1	2.4	2.6	4.14±43%
Dust AOD	0.029	0.029	0.029	0.032	0.029	0.033	0.023

*Note. The numbers in parentheses are calculated dry (or wet) deposition rate in unit of day^{-1} , defined as dry (or wet) deposition flux divided by burden*365 in Textor et al. (2006). Also shown are the model outputs from CAM5 (Scanza et al., 2015). The means and normalized standard deviations (in %) of the “Other studies” are taken from Liu et al. (2012) except for dust AOD from Huneus et al. (2011)*

Table 5 Annual and global mean radiation budgets in E3SMv1 (LRes, LResT, LResT-HRtuned, HResT and HResT*). Also shown are the global DAOD and AOD associated with the estimated radiative fluxes.

	DAOD	AOD	TOA ($W m^{-2}$)			Atmosphere ($W m^{-2}$)			Surface ($W m^{-2}$)		
			SW	LW	NET	SW	LW	NET	SW	LW	NET
LRes	0.029	0.142	-0.16	0.08	-0.08	1.35	-0.34	1.01	-1.51	0.42	-1.09
LResT	0.029	0.141	-0.52	0.1	-0.42	0.68	-0.44	0.24	-1.20	0.54	-0.65
LResT-HRtuned	0.038	0.149	-0.74	0.14	-0.6	0.99	-0.65	0.35	-1.73	0.79	-0.95
HResT	0.04	0.147	-0.73	0.16	-0.58	1.08	-0.71	0.37	-1.81	0.87	-0.95
HResT*	0.029		-0.53	0.12	-0.42						

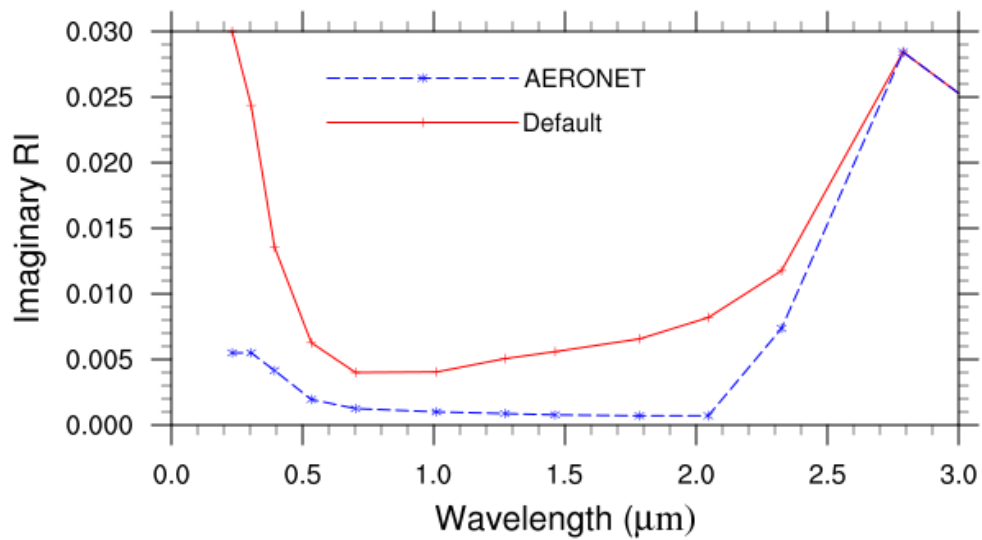


Figure 1. Dust imaginary refractive indices (RI) in the default E3SM model and sensitivity studies of this work based on the AERONET measurements

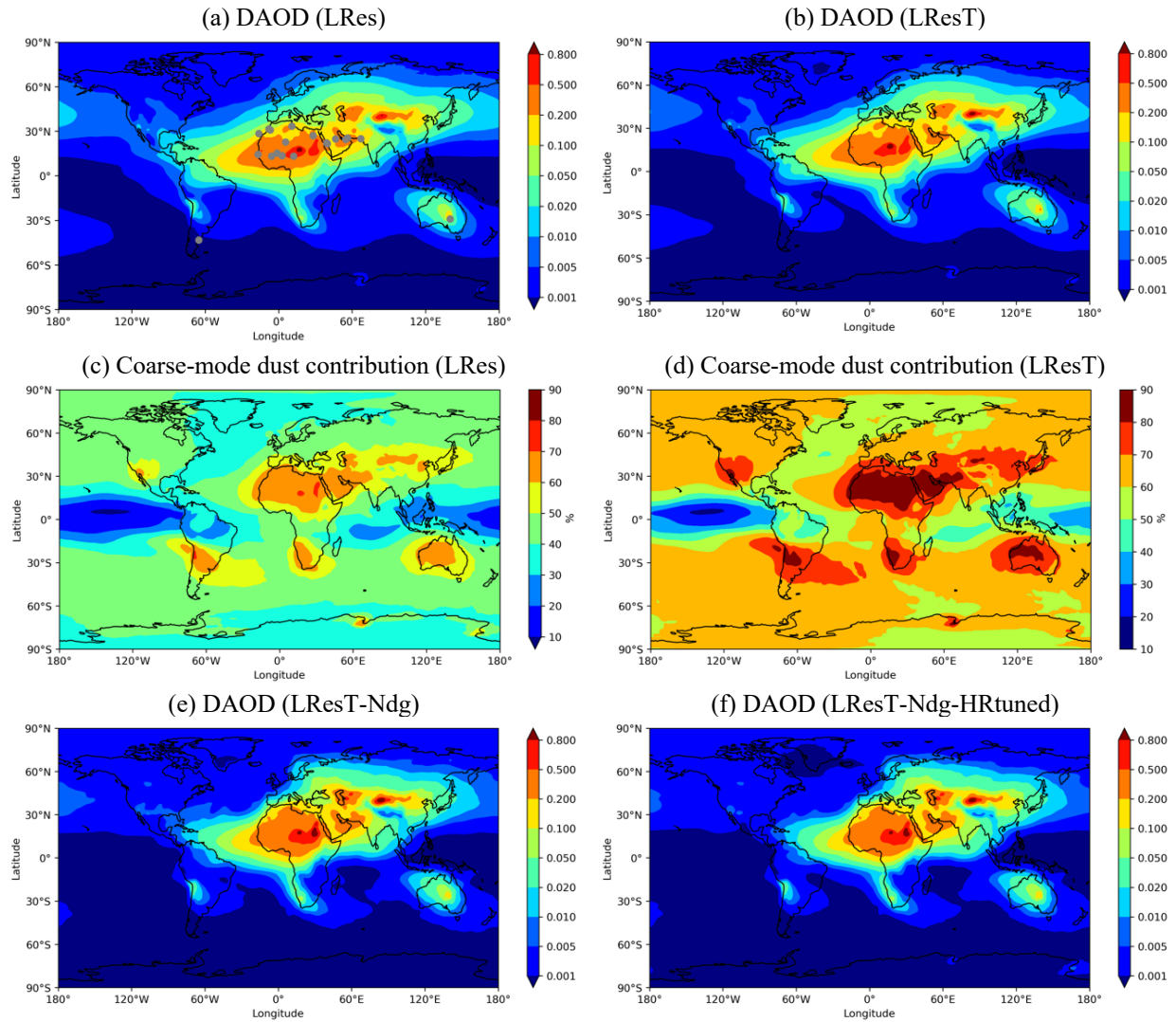


Figure 2. Annual mean dust aerosol optical depth (DAOD) at 550nm predicted by the low-resolution E3SMv1 with the (a) default configuration (LRes) and (b) updated dust physics (LResT). Contribution (%) of the coarse-mode dust in total DAOD is shown for (c) LRes and (d) LResT, respectively. Also shown are the annual mean DAOD distributions from the two sensitivity studies: (e) LResT-Ndg and (f) LResT-Ndg-HRtuned. Grey circles in the panel (a) indicate the 19 ‘dusty’ AERONET sites selected

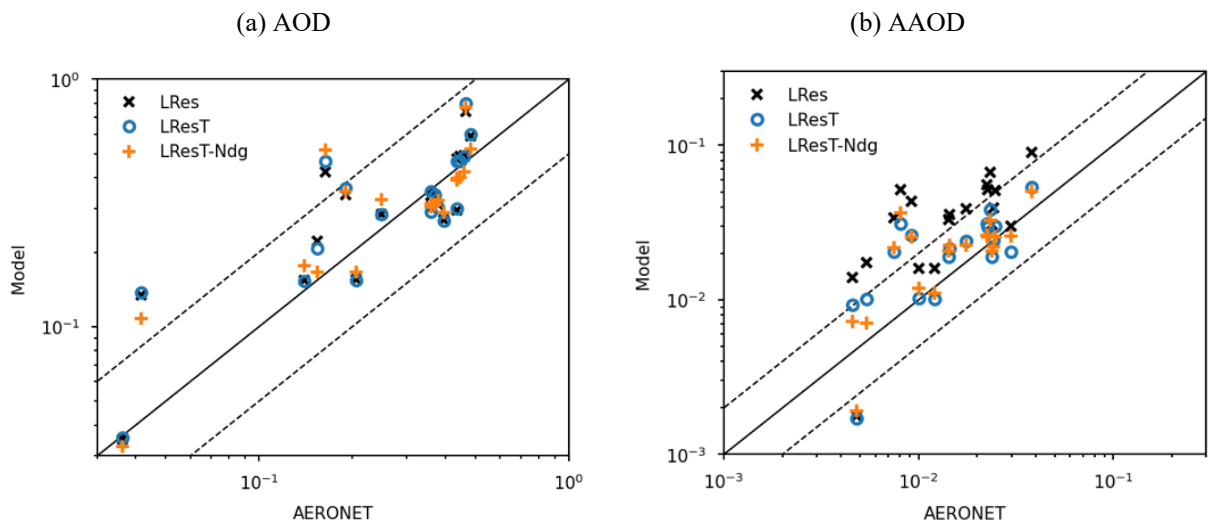


Figure 3. Annual mean (a) AOD and (b) AAOD comparison with the AERONET data over the selected dusty sites. Results from the LRes (cross symbols), LResT (open circles), and LResT-Ndg (plus symbols) simulations are shown. The black solid line represents the 1:1 line and the dash lines are for the 1:2 and 2:1 ratios

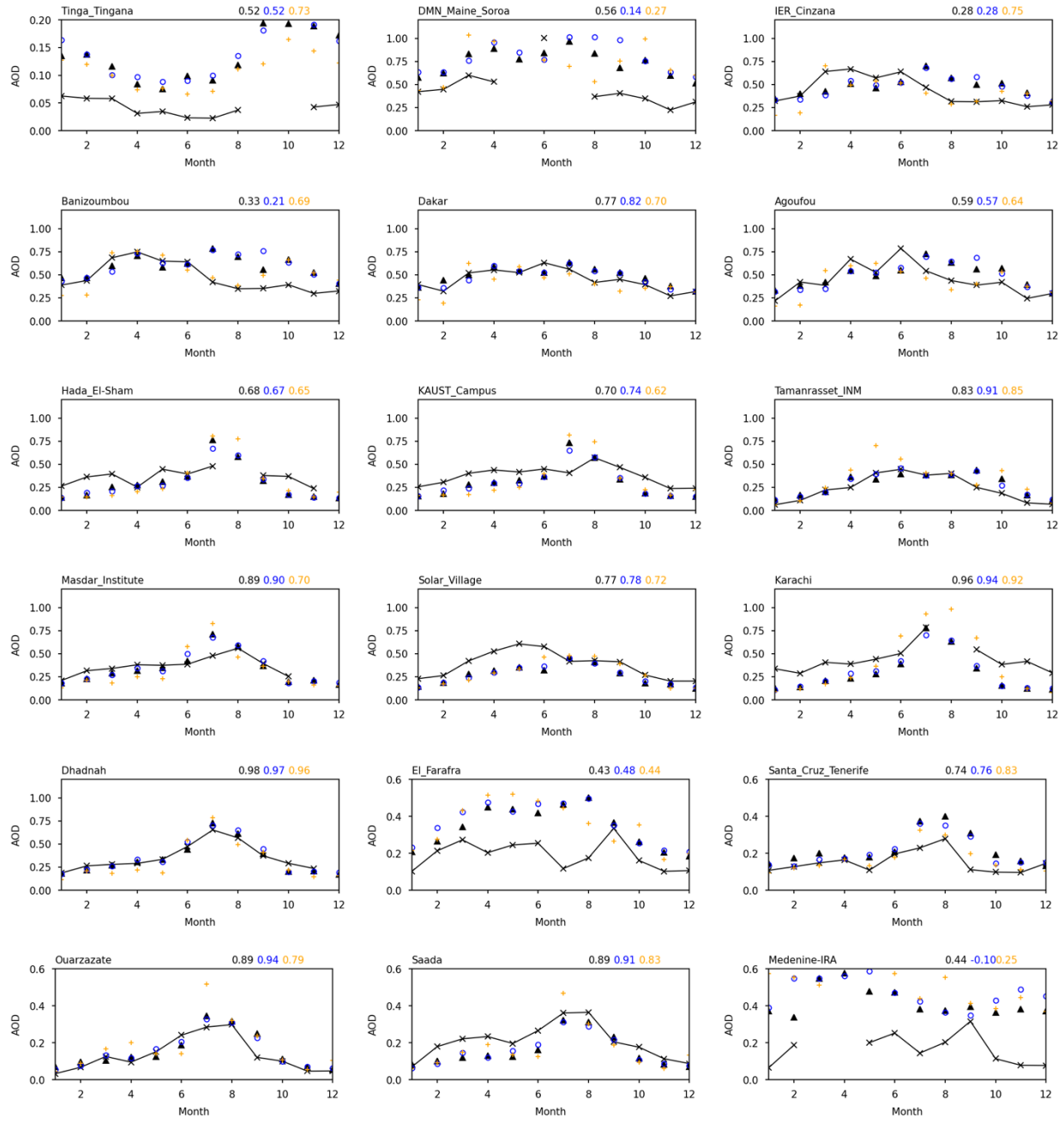


Figure 4. Seasonal variations of monthly AODs over the 18 dusty AERONET sites simulated by LRes (triangle), LResT (blue circle), and LResT-Ndg (orange plus), compared with the AERONET data (line with cross symbols). The site name and calculated Pearson correlation coefficients between LRes (black), LResT (Blue), LResT-Ndg (orange) and observations are shown on top of each panel. The AERONET site information is given in Table 2

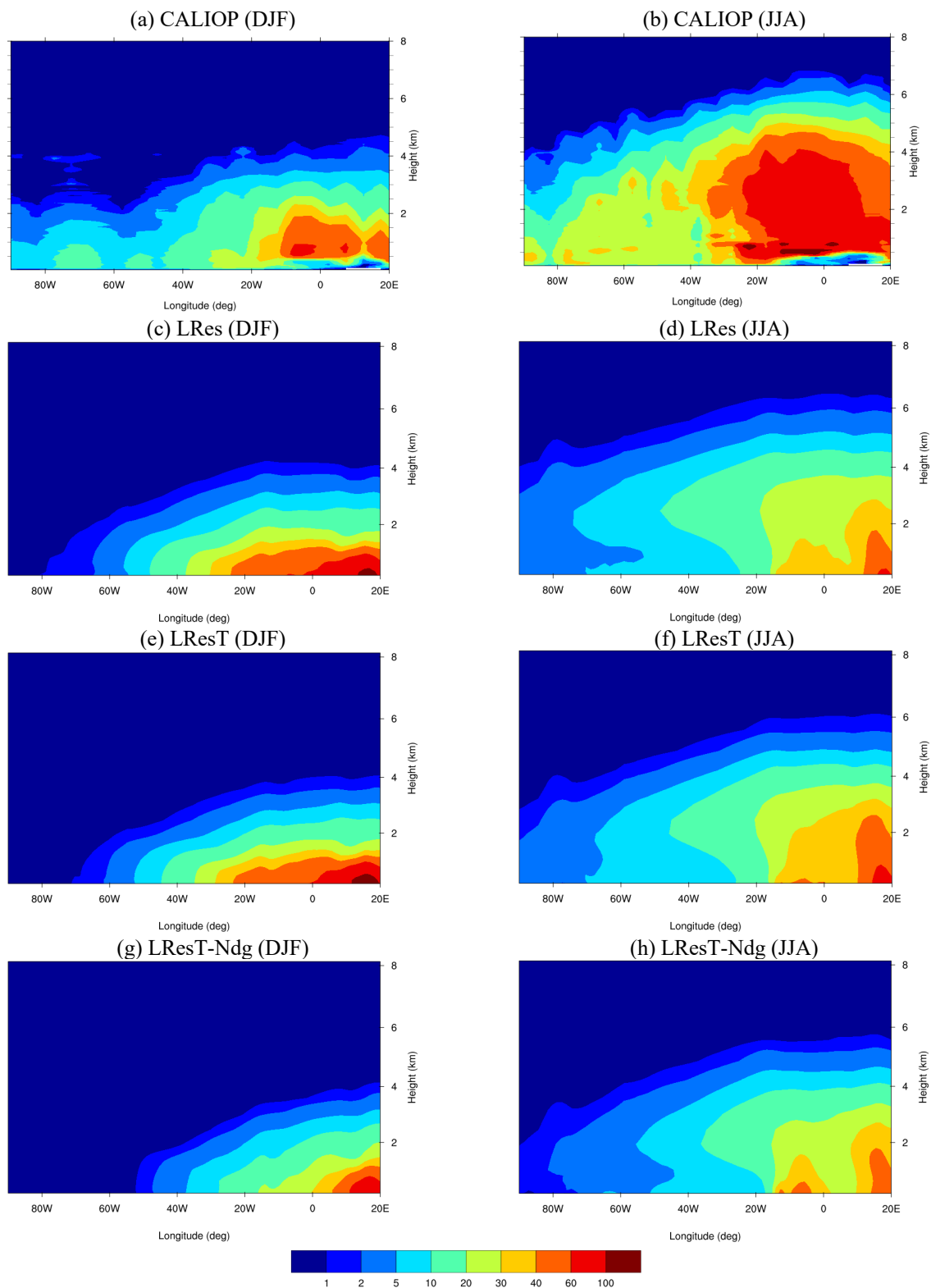


Figure 5. Crosssection of dust extinctions (Mm^{-1}) averaged between 0 and 30°N for winter (DJF: December-January-February), and summer (JJA: June-July-August), as shown in (a) and (b) for the CALIOP retrievals in year 2010, compared with the E3SM simulations in (c) and (d) from LRes, (e) and (f) from LResT, and (g) and (h) from LResT-Ndg

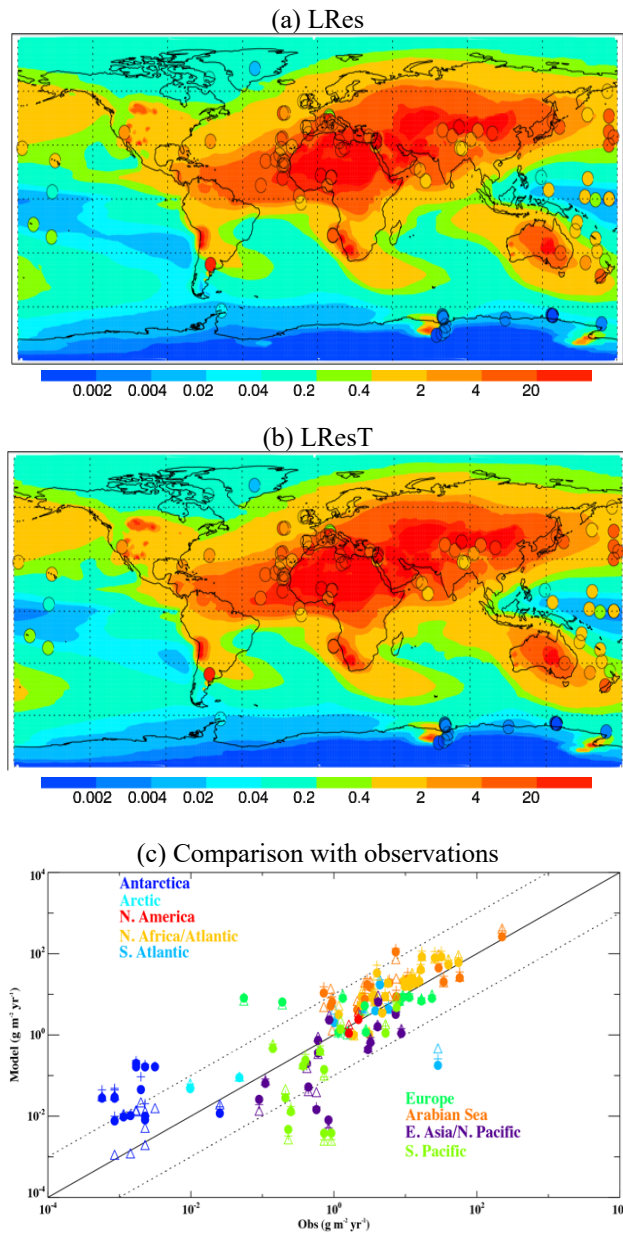


Figure 6. Spatial distribution of annual dust deposition flux ($\text{g m}^{-2} \text{yr}^{-1}$) from (a) LRes and (b) LResT. Observational data over 108 locations are overlaid by filled circles with values shown in the same colour scale. Panel (c) compares the model results from LRes (solid circles), LResT (plus symbols), and HRes (open triangles) with the data at the observational sites. The black solid line represents the 1:1 line and the dash lines are for the 1:10 and 10:1 ratios

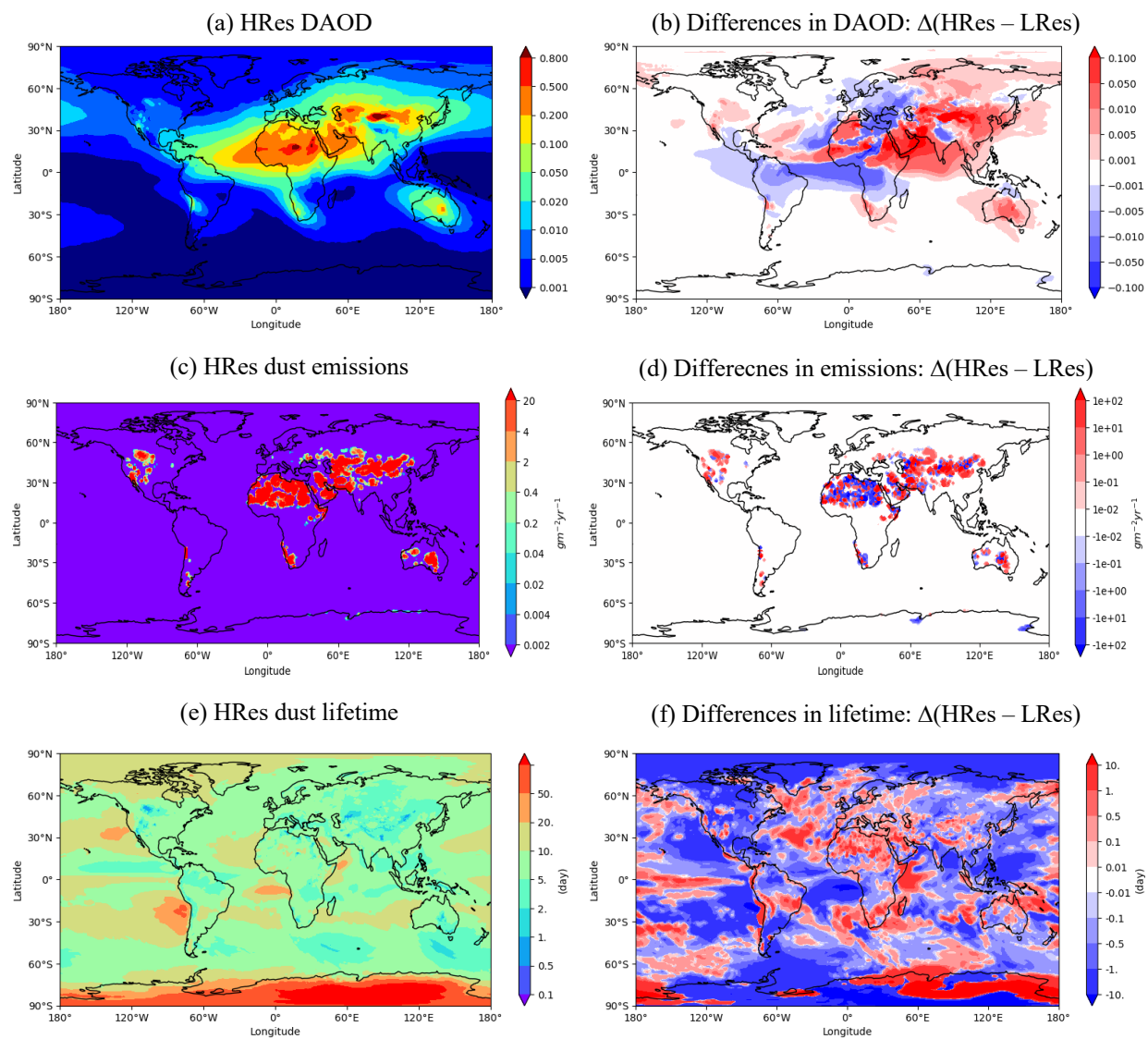


Figure 7. HRes simulations of (a) annual mean DAOD at 550nm, (c) dust emissions ($\text{g m}^{-2} \text{yr}^{-1}$), and (e) lifetime (day). Also shown are the differences between the HRes and LRes simulations in (b) DAOD, (d) dust emissions ($\text{g m}^{-2} \text{yr}^{-1}$), and (f) lifetime (day)

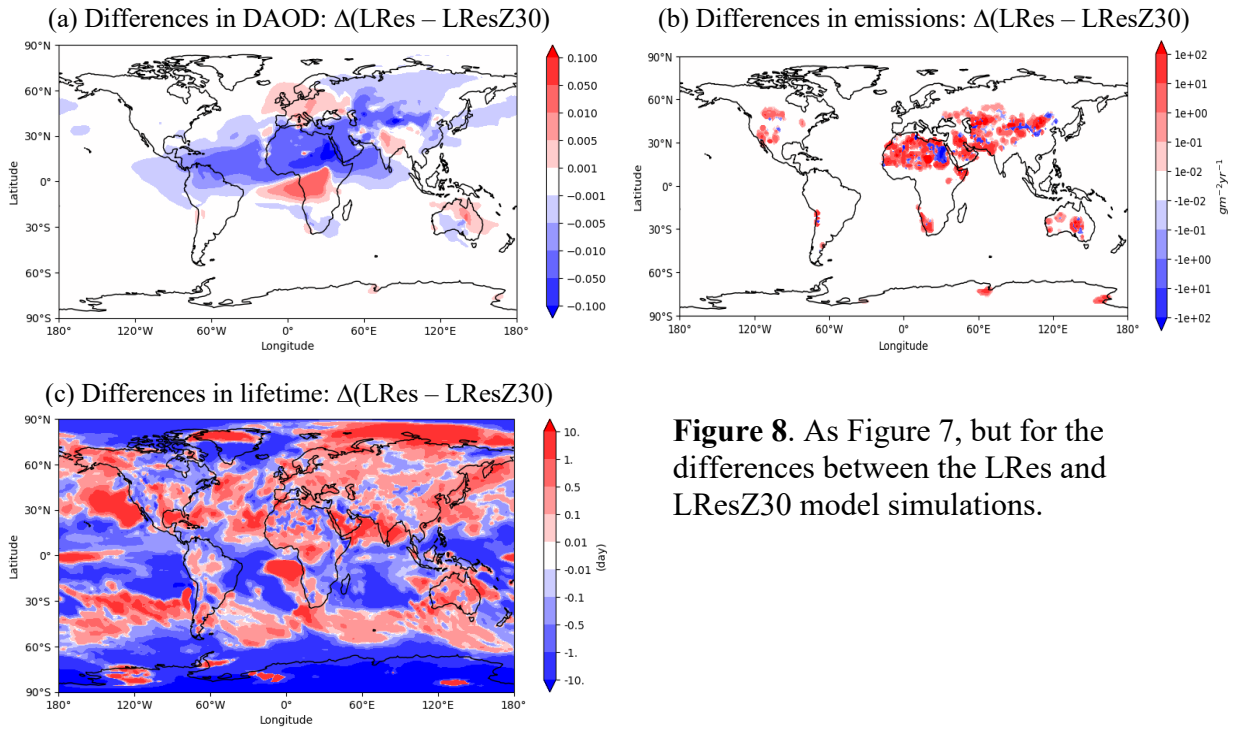


Figure 8. As Figure 7, but for the differences between the LRes and LResZ30 model simulations.

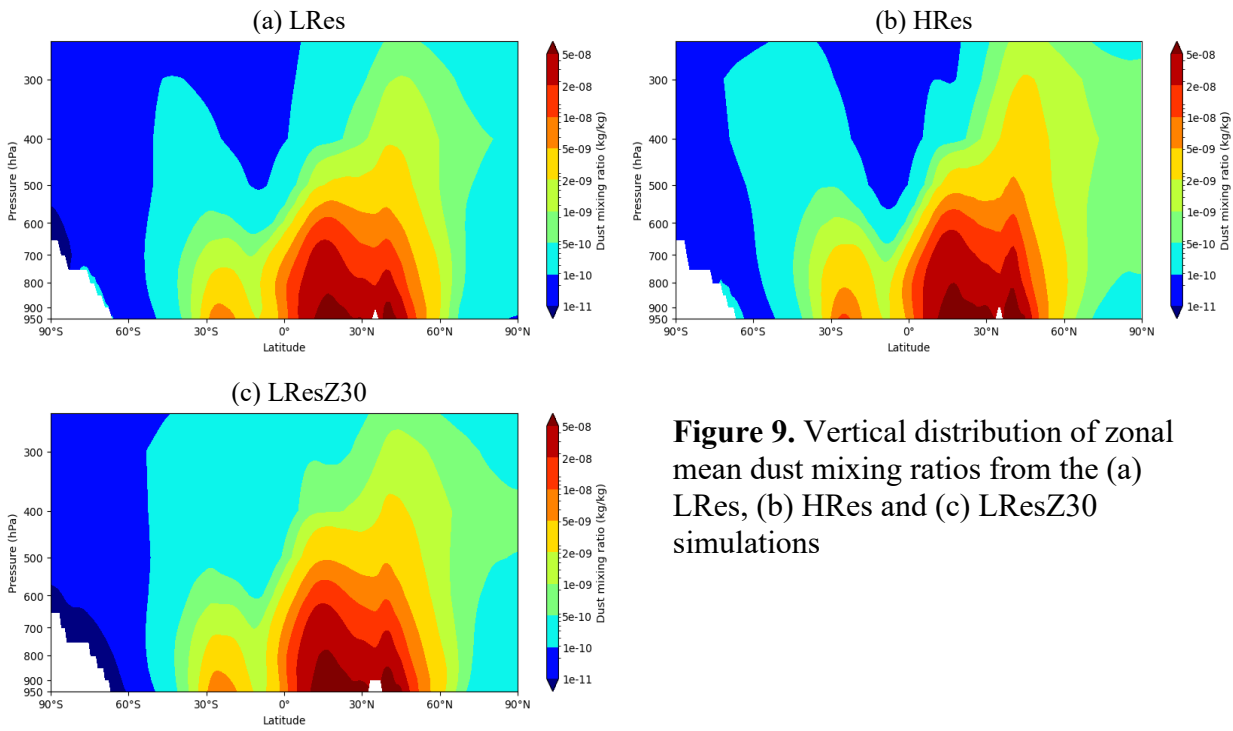


Figure 9. Vertical distribution of zonal mean dust mixing ratios from the (a) LRes, (b) HRes and (c) LResZ30 simulations

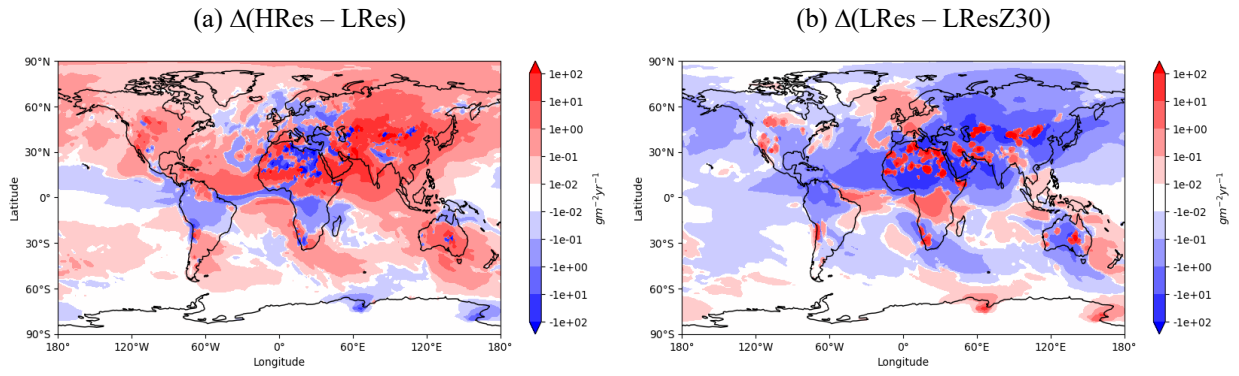


Figure 10. Differences in simulated annual dust deposition fluxes ($\text{g m}^{-2} \text{yr}^{-1}$) between (a) HRes and LRes: $\Delta(\text{HRes} - \text{LRes})$ and (b) LRes and LResZ30: $\Delta(\text{LRes} - \text{LResZ30})$

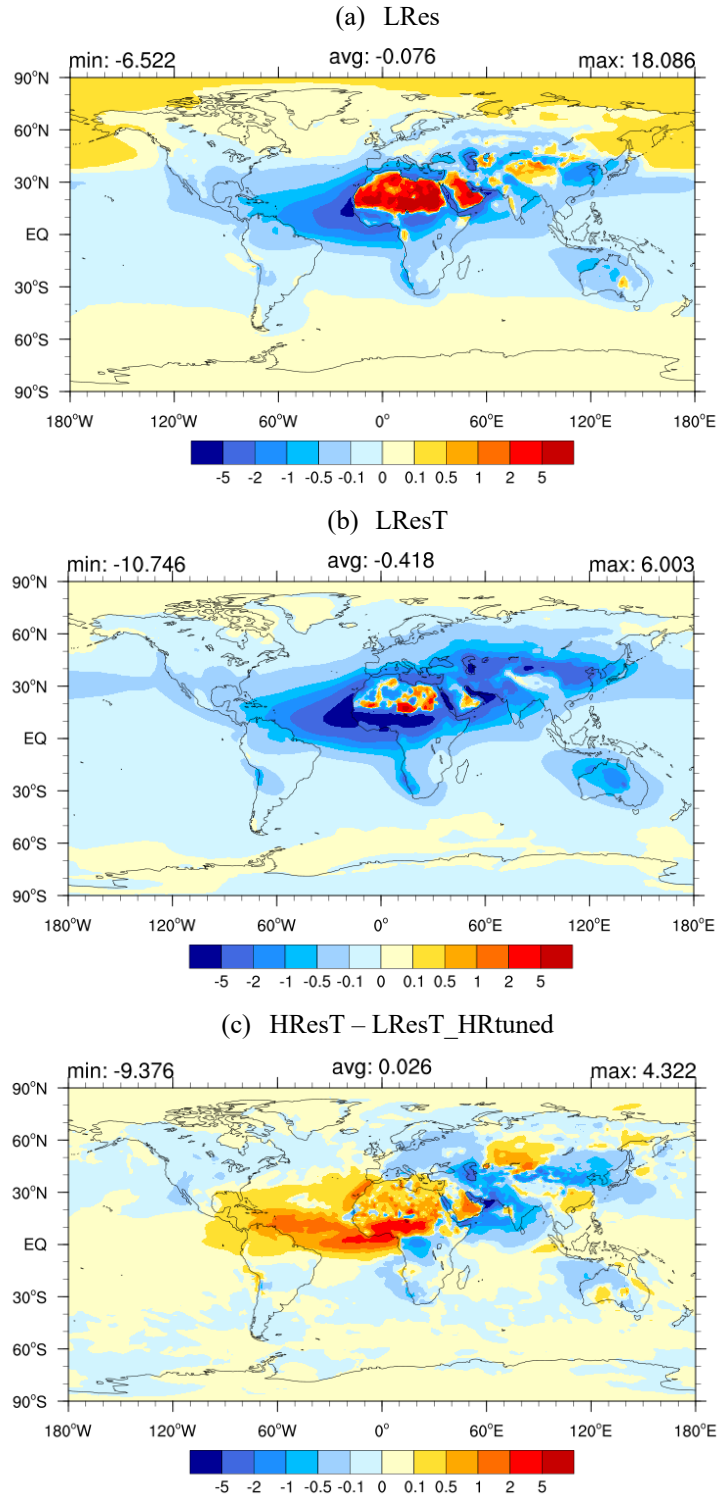


Figure 11. Dust direct radiative effect (W m^{-2}) at the top of the atmosphere from (a) LRes (EAMv1 low resolution), (b) LResT (this work), and (c) HResT-LResT_HRtuned (impact of higher horizontal resolution)

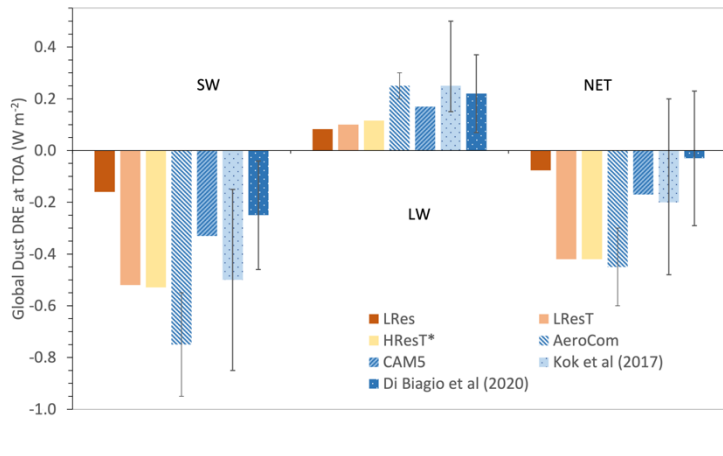


Figure 12. Comparison of the estimated dust direct radiative effects (DRE: $W m^{-2}$) at the top of the atmosphere (TOA) for for the shortwave (SW), longwave (LW), and net effects (NET), respectively, from the E3SM simulations (LRes, LResT, and HResT*). HResT* denotes the HResT DREs, whose values are normalized to the LRes DAOD. Also shown are the results from CAM5 (Scanza et al., 2015), Di Biagio et al. (2020), and Kok et al. (2017) which also include the published AeroCom model estimates